JAERI 1334

JAERI 1334

WSPEEDI (Worldwide Version of SPEEDI) : A Computer Code System for the Prediction of Radiological Impacts on Japanese due to a Nuclear Accident in Foreign Countries

September 1995

日 本 原 子 力 研 究 所

Japan Atomic Energy Research Institute

日本原子力研究所研究成果編集委員会

委員長　市　川　逵　生（理事）

委　　員

新井　英彦（環境・資源利用研究部）
一色　正彦（研究炉部）
太田　　充（核融合工学部）
岡田　漱平（放射線高度利用センター）
落合　政昭（原子力船研究開発室）
菊地　　章（ホット試験室）
鴻坂　厚夫（安全性試験研究センター）
西堂　雅博（核融合装置試験部）
白石　浩二（燃料研究部）
鈴木　紀男（炉心プラズマ研究部）
竹下　　功（ＮＵＣＥＦ試験室）
田中　利幸（高温工学試験研究炉開発部）
棚瀬　正和（アイソトープ部）
千原　順三（材料研究部）
新保　利定（材料試験炉部）
原見　太幹（大型放射光施設開発室）
平林　孝圀（バックエンド技術部）
平松　伸章（技術情報部）
藤根　幸雄（燃料サイクル安全工学部）
藤村　　薫（先端基礎研究センター）
松鶴　秀夫（環境安全研究部）
水本　元治（原子炉工学部）
武藤　　康（高温工学部）
森田　洋右（材料開発部）
吉田　　真（保健物理部）
渡邊　　勉（企画室）

Japan Atomic Energy Research Institute

Board of Editors

Michio Ichikawa (Chief Editor)

Hidehiko Arai
Sachio Fujine
Nobuaki Hiramatsu
Atsuo Kohsaka
Yosuke Morita
Masaaki Ochiai
Masahiro Saido
Isao Takeshita
Tsutomu Watanabe
Junzo Chihara
Taikan Harami
Masahiko Isshiki
Hideo Matsuzuru
Yasushi Mutou
Sohei Okada
Hirotsugu Shiraishi
Toshiyuki Tanaka
Makoto Yoshida
Kaoru Fujimura
Takakuni Hirabayashi
Akira Kikuchi
Motoharu Mizumoto
Toshisada Niibo
Mitsuru Ohta
Morio Suzuki
Masakazu Tanase

JAERIレポートは，日本原子力研究所が研究成果編集委員会の審査を経て不定期に公刊している研究報告書です。

入手の問合わせは，日本原子力研究所技術情報部情報資料課（〒319-11 茨城県那珂郡東海村）あて，お申込み下さい。なお，このほかに財団法人原子力弘済会資料センター（〒319-11 茨城県那珂郡東海村日本原子力研究所内）で複写による実費頒布をおこなっております。

JAERI reports are reviewed by the Board of Editors and issued irregularly.

Inquiries about availability of the reports should be addressed to Information Division, Department of Technical Information, Japan Atomic Energy Research Institute, Tokai-mura, Naka-gun, Ibaraki-ken 319-11, Japan.

©Japan Atomic Energy Research Institute, 1995

編集兼発行　日本原子力研究所
印　　刷　日立高速印刷㈱

WSPEEDI(Worldwide Version of SPEEDI): A Computer Code System for the Prediction of Radiological Impacts on Japanese due to a Nuclear Accident in Foreign Countries

Masamichi CHINO, Hirohiko ISHIKAWA*, Hiromi YAMAZAWA,
Haruyasu NAGAI and Shigeru MORIUCHI

Department of Environmental Safety Research,
Tokai Research Establishment,
Japan Atomic Energy Research Institute
Tokai-mura, Naka-gun, Ibaraki-ken, Japan
(Received March 7, 1995)

Abstract

A computer code system has been developed for near real-time dose assessment during radiological emergencies. The system WSPEEDI, the worldwide version of SPEEDI (System for Prediction of Environmental Emergency Dose Information) aims at predicting the radiological impact on Japanese due to a nuclear accident in foreign countries. WSPEEDI consists of a mass-consistent wind model WSYNOP for large-scale wind fields and a particle random walk model GEARN for atmospheric dispersion and dry and wet deposition of radioactivity. The models are integrated into a computer code system together with a system control software, worldwide geographic database, meteorological data processor and graphic software. The performance of the models has been evaluated using the Chernobyl case with reliable source terms, well-established meteorological data and a comprehensive monitoring database. Furthermore, the response of the system has been examined by near real-time simulations of the European Tracer Experiment (ETEX), carried out over about 2,000 km area in Europe.

Keywords: Computer code, Nuclear emergency, Atmosphere, Accidental release, Prediction, Long-range transport, Real-time, SPEEDI, WSPEEDI, Chernobyl

---

* Disaster Prevention Res. Inst., Kyoto University, Gokasyo, Uji-shi, JAPAN

WSPEEDI (世界版SPEEDI)：国外原子力事故に伴う日本への放射能影響予測のための緊急時対応システム

日本原子力研究所東海研究所環境安全研究部

茅野政道・石川裕彦*・山澤弘実・永井晴康・森内　茂

（１９９５年３月７日　受理）

要　　旨

国外原子力施設事故時に、実時間被曝線量評価により防災対策を支援する計算システムWSPEEDIを開発した。SPEEDIの世界版であるWSPEEDIは、国外の原子力事故に伴う日本への放射能影響予測を目的としている。WSPEEDIは、広域風速場予測のための質量保存風速場モデルWSYNOPと、放射能の長距離拡散，地表面沈着及び被曝線量評価のためのランダムウォークモデルGEARNから構成される。計算モデルは、システム制御機能、世界地図データベース、気象データ処理機能、図形出力機能等と共にシステム化されている。計算モデルは信頼性の高い放出源情報、気象情報、モニタリングデータを集約したチェルノブイル事故データベースを用いて検証された。さらに、緊急時システムとしての対応能力が、ヨーロッパ大陸の約2,000kmスケールで行われたヨーロッパ広域拡散実験のリアルタイムシミュレーションにより評価された。システムは、現在、ほぼ実用段階に達している。

* 京都大学防災研究所，宇治市五ケ庄

CONTENTS

1. Introduction 1
1.1 Background 1
1.2 Outline of WSPEEDI 2
2. Numerical Models 4
2.1 Coordinates and Grid System 5
2.2 Wind Field Model WSYNOP 6
2.2.1 Estimation of initial guess 6
2.2.2 Variational analysis 7
2.3 Concentration and Dose Model GEARN 10
2.3.1 Modeling of atmospheric dispersion 10
2.3.2 Air concentration 12
2.3.3 Deposition 12
2.3.4 Radiological doses 13
3. System Integration 15
3.1 Computer Network and Its Functions 15
3.2 System Control Software 16
3.3 Meteorological Data Processor 18
3.4 Databases 20
3.5 Graphical Output 22
4. Verification Studies 27
4.1 Simulation of the Chernobyl Accident 27
4.1.1 Framework of calculation 27
4.1.2 Results and discussion 29
4.1.3 Summary 36
4.2 Real-time Operation for European Tracer Experiment(ETEX) 36
4.2.1 Outline of ETEX 36
4.2.2 Application of WSPEEDI to ETEX 39
4.2.3 Summary 49
5. Concluding Remarks 50

Acknowledgment 52
References 53

目　　次

1. 緒言 …… 1
1.1 背景 …… 1
1.2 WSPEEDI の概要 …… 2
2. 数値モデル …… 4
2.1 座標系と計算格子 …… 5
2.2 風速場モデル WSYNOP …… 6
2.2.1 初期値推定法 …… 6
2.2.2 変分解析 …… 7
2.3 濃度・線量モデル GEARN …… 10
2.3.1 大気拡散モデル …… 10
2.3.2 大気中濃度 …… 12
2.3.3 沈着量 …… 12
2.3.4 被曝線量 …… 13
3. システム化 …… 15
3.1 計算機ネットワークと機能 …… 15
3.2 システム制御機能 …… 16
3.3 気象データ処理機能 …… 18
3.4 データベース …… 20
3.5 図形出力 …… 22
4. 検証研究 …… 27
4.1 チェルノブイル事故シミュレーション …… 27
4.1.1 計算の概要 …… 27
4.1.2 結果と検討 …… 29
4.1.3 まとめ …… 36
4.2 ヨーロッパ広域拡散実験（ETEX）の実時間予測 …… 36
4.2.1 ETEXの概要 …… 36
4.2.2 WSPEEDI の ETEX への適用 …… 39
4.2.3 まとめ …… 49
5. 結　　言 …… 50

謝　辞 …… 52
参考文献 …… 53

List of Tables

Table 1 The values of parameters used in Eq.(34).
Table 2 Typical CPU time and memory size.
Table 3 The major commands to operate WSPEEDI.
Table 4 Meteorological data given from the GPV.
Table 5 Databeses and their contents.
Table 6 Numerical and graphical outputs.
Table 7 Comparison of plume arrival date at several European countries.
Table 8 Comparison of calculated and measured surface deposition (kBq/m^2) accumulated until May 10.
Table 9 Specification of topographical database used for ETEX.
Table 10 The progress with time of near real-time response on Run 1.
Table 11 The progress with time of near real-time response on Run 2.

List of Figures

Fig. 1 Difference of objective scale between SPEEDI and WSPEEDI.
Fig. 2 The main soft- and hardwares which consist of WSPEEDI.
Fig. 3 Computational flow of WSPEEDI.
Fig. 4 Flowchart of a three-dimensional mass-consistent wind field model WSYNOP.
Fig. 5 Illustration of a particle random walk model GEARN.
Fig. 6 Schematic diagram to explain the interpolation of wind vectors on the grids to the particle position.
Fig. 7 The computer network of WSPEEDI.
Fig. 8 The primary functions of modules and computers of WSPEEDI.
Fig. 9 Some examples of user-interface menus to operate WSPEEDI;
(a) the menu to input accident site,
(b) the menu to submit wind field calculation.
Fig. 10 Diagram of world meteorological data flow to WSPEEDI.
Fig. 11 Three geographical regions supported by WSPEEDI,
(a) the Asian, (b) European and (c) hemispheric regions.
Fig. 12 Some examples of new graphic outputs implemented in the workstation;
(a) the wind field near the surface over Europe,
(b) air concentration calculated in the Asian region, and
(c) surface deposition of ^{137}Cs during the Chernobyl accident.
Fig. 13 The computational area for the Chernobyl simulation, which is denoted by broken lines together with the distribution of meteorological observatories.
Fig. 14 The daily release rate of ^{137}Cs during the accident used for calculations.
Fig. 15 The evolution of surface air concentration at 0000 GMT from 27 April to 8 May.
Fig. 16 Movement of marker particles which represent ^{137}Cs released on (a) 26 April and (b) 4 May.
Fig. 17 Calculated surface air concentrations compared with measurements at several locations.
Fig. 18 Correlation of daily averaged surface air concentrations between the measured and the calculated.
Fig. 19 Calculated deposition of ^{137}Cs accumulated until 0000 GMT, 11 May 1986.
Fig. 20 Study area of ETEX, encompassed the European region between 4° w to 25° E and 44° N to 64° N approximately. Black circles show tracer samplers.
Fig. 21 The source information on Run 1 and Run 2 sent by facsimile from the ETEX evaluation team.
Fig. 22 The data communications flow used by WSPEEDI for ETEX.
Fig. 23 The results of Set 1 in Run 1, which were based on the forecast data 23_12, Oct.;
(a) - (c) : predicted wind fields near the surface at 1200 GMT, 23, 24 and 25 Oct., and
(d) - (f) : predicted air concentrations at the ground level at T_0+24 (16 GMT, 24 Oct.), T_0+48 (16 GMT, 25 Oct.) and T_0+60 (04 GMT, 26 Oct.). The contour values are 10^{-1}, 10^{-2}, 10^{-3}, 10^{-4} and 10^{-5} ng/m^3 from the inside.
Fig. 24 The final results, Set 6 in Run 1, improved by analyzed wind fields.
Fig. 25 Comparison of the air concentrations at the ground level at T_0+60 from Set 1 to 6.

Fig. 26 The results of Set 1 in Run 2, which were based on the forecast data 14_12, Nov.;
(a) - (c) : predicted wind fields near the surface at 1200 GMT, 14, 15 and 16 Nov., and
(d) - (f) : predicted air concentrations at the ground level at T_0+24 (15 GMT, 15 Nov.), T_0+48 (15 GMT, 16 Nov.) and T_0+60 (03 GMT, 17 Nov.).

Fig. 27 Wind fields (Set 1) at a height of 500 m above the ground at 0000 GMT, 16 Nov.

Fig. 28 The final results, Set 6 in Run 2, improved by analyzed wind fields.

This is a blank page.

1. Introduction

1.1 Background

The development of a full-scale off-site countermeasure program against the accidental release of radioactivity was initiated in Japan by the TMI-2 reactor accident in the United States in March 1979. Immediately after the accident, the Japanese Government set up a national scale support program for local governments who are responsible for taking public protective actions during radiological emergencies.

Every possible action to assure the safety of the surrounding population is based on the 'Report on Countermeasures against a Nuclear Accident'[1] issued by the Japan Nuclear Safety Commission. This report describes an emergency planning zone, off-site monitoring procedures, action levels for sheltering, evacuation, etc. In addition, off-site monitoring procedures in emergency situations are explained in detail in the 'Guideline for Emergency Monitoring'[2] issued by the same commission. On the basis of this guideline, local governments have been preparing local emergency monitoring plans and equipment, in addition to telemetry systems for routine monitoring of the dose rates in the air around sites. The first version of the guideline also indicated the use of a computer-based dose estimation using the Gaussian plume model for the selection of an emergency monitoring area. However, because it is evident that the Gaussian plume model is inadequate to simulate time-dependent atmospheric dispersion over complex terrain, the necessity for more reliable numerical predictions has been identified. In response to such requirements, the Japan Atomic Energy Research Institute (JAERI) has developed a suite of software for SPEEDI (System for Prediction of Environmental Emergency Dose Information) [3] which is an assembly of new atmospheric dispersion models, databases, man-machine interfaces, graphics, etc., and the Science and Technology Agency (STA) subsequently constructed a data communications network[4] for the practical use of SPEEDI. In recognition of the completion of the network, the Japan Nuclear Safety Commission revised the guideline to adopt SPEEDI for near real-time analysis of air concentrations, dose distributions, etc. The latest guideline, revised in 1992, suggests that experts of the local emergency headquarters should estimate off-site contamination situations based on environmental monitoring by local governments and the results predicted by SPEEDI supplied from the national emergency headquarters.

Although an off-site countermeasure program against domestic local range accidents has been established by national and local governments, the task of designing a concrete national scale countermeasure program against overseas accidents still remains. However, after the Chernobyl accident in former Soviet Union in April 1986, the necessity of having a computational system to predict environmental consequences of a large-scale nuclear accident has been recognized in many countries as well as Japan. The development of new long-range transport models and/or application of existing air pollution modeling techniques to environmental radioactivity issues was started in many institutes after the accident. Some of the early studies were presented at EURASAP (European Association of Air Pollution) meeting in Vienna in 1988[5]. This necessity was also recognized by international agencies such as IAEA (International Atomic Energy Agency), WMO (World Meteorological Organization) and CEC (Commission of the European Communities). These agencies sponsored an international cooperative study, called ATMES (Atmospheric Transport Model Evaluation Study)[6], in which twenty-one institutions from fourteen countries participated. In

ATMES, the performance of various different models was evaluated using European monitoring data during the Chernobyl accident.

During the emergency situation of Chernobyl, JAERI has predicted the dispersion of radionuclides over Europe[7] by using SPEEDI, which was slightly modified to simulate the long-range transport on a regional scale. Following this, under the national research program by the Nuclear Safety Commission, a new technical capability, WSPEEDI (Worldwide version of SPEEDI), has been developed to predict the radiological impact on Japanese due to a nuclear accident in foreign countries.

1.2 Outline of WSPEEDI

During a nuclear emergency, it is difficult to determine the total feature of radioactive clouds from the limited real-time radiation monitoring data. Furthermore, although some part of radioactivity in the atmosphere is deposited on the ground by air turbulence and precipitation, it takes a long time to perform a full-scale survey over a contaminated area. These facts indicate that computational simulation with a long-range transport model might be only practical measure of tracing a radioactive cloud during the early stage of an accident. The simulation of transport and deposition of radionuclides provides tentative information in support of the establishment of early countermeasures to mitigate radiological consequences, until a full-scale survey is completed.

To meet these requirements, WSPEEDI has been designed to execute near real-time estimating of the long-range atmospheric transport and deposition of airborne radioactivity in a synoptic or hemispheric area. Here, "near real-time" means that the atmospheric transport of radionuclides is calculated by using present and forcast meteorological data to estimate present and near future contamination areas. WSPEEDI is based on SPEEDI. The difference between SPEEDI and WSPEEDI is schematically illustrated in **Fig.1**. The abscissa and ordinate represent the horizontal and vertical scales, respectively. The coverage of SPEEDI and WSPEEDI is shown by thick lines together with major nuclear energy related episodes. As shown in the figure, WSPEEDI is designed to

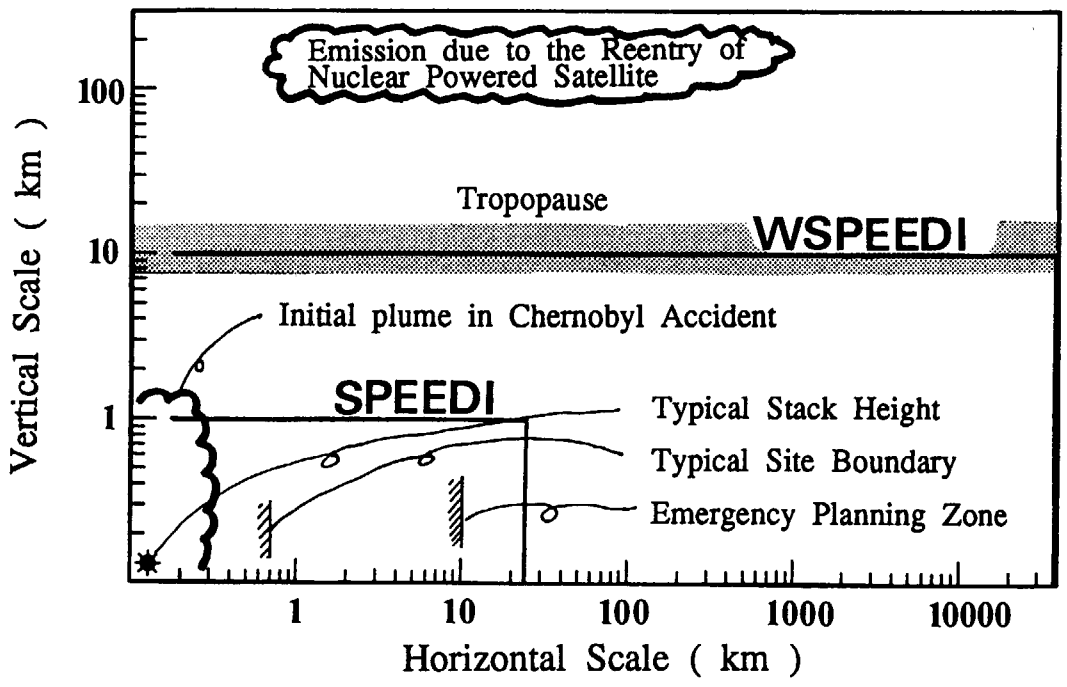

Fig.1 Difference of objective scale between SPEEDI and WSPEEDI.

simulate the long-range transport of radionuclides up to the hemisphere. The vertical dimension of the computational domain is extended to the top of troposphere (~ 10 km). WSPEEDI consists of a mass-consistent wind model (WSYNOP)[8] for large-scale wind fields and a particle random walk model (GEARN)[9] for atmospheric dispersion and dry and wet deposition of radioactivity. The combination of models, WSYNOP/GEARN, is formulated with a map coordinate horizontally and a terrain-following coordinate vertically. The profile of air density is also considered so that they can be applied to a deep layer of the atmosphere. **Figure 2** shows the structure of WSPEEDI. To make a prompt response to an emergency situation immediately, WSPEEDI basically inherited the integrated computational environment of SPEEDI, e.g., man-machine interface, worldwide geographic database, processor to handle enormous amount of worldwide meteorological data, graphics and so on. The performance of the models has been evaluated using the Chernobyl case with reliable source terms, well-established meteorological data and a comprehensive monitoring database. Furthermore, the response of the system has been examined by near real-time operation of the European Tracer Experiment (ETEX), carried out over about a 2,000 km area in Europe.

In this paper, details of numerical models are given in Chapter 2. The model supporting functions, e.g., graphics, databases, etc., are described in Chapter 3, followed by verification studies in Chapter 4 and the paper is finalized with some conclusions in Chapter 5.

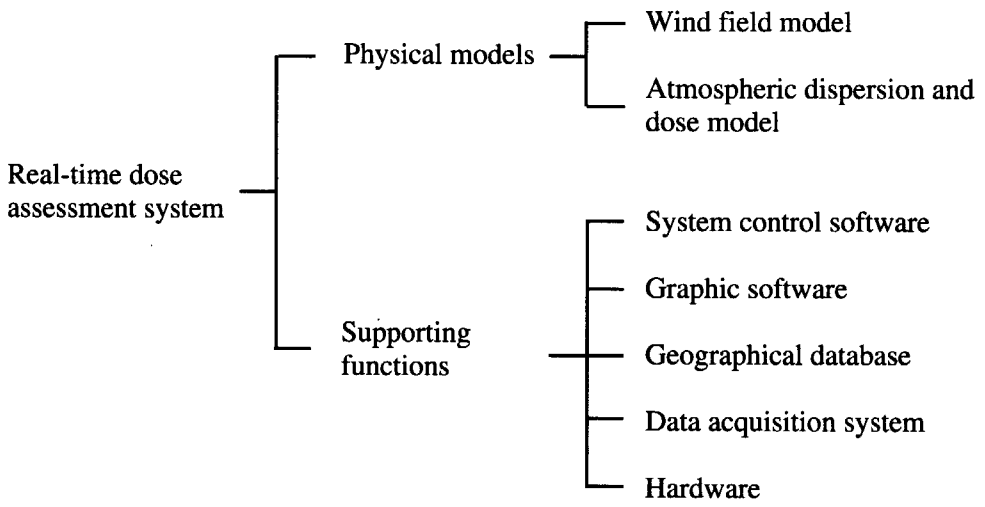

Fig. 2 The main soft- and hardwares which consist of WSPEEDI.

2. Numerical Models

WSPEEDI consists of a mass-consistent wind model, WSYNOP, for large-scale wind fields and a particle random walk model, GEARN, for atmospheric dispersion, dry and wet deposition of radioactivity, and dose calculations. These models can take account of the complex source, terrain conditions, and non-uniform and non-steady atmosphere. **Figure 3** denotes the computational flow of these models.

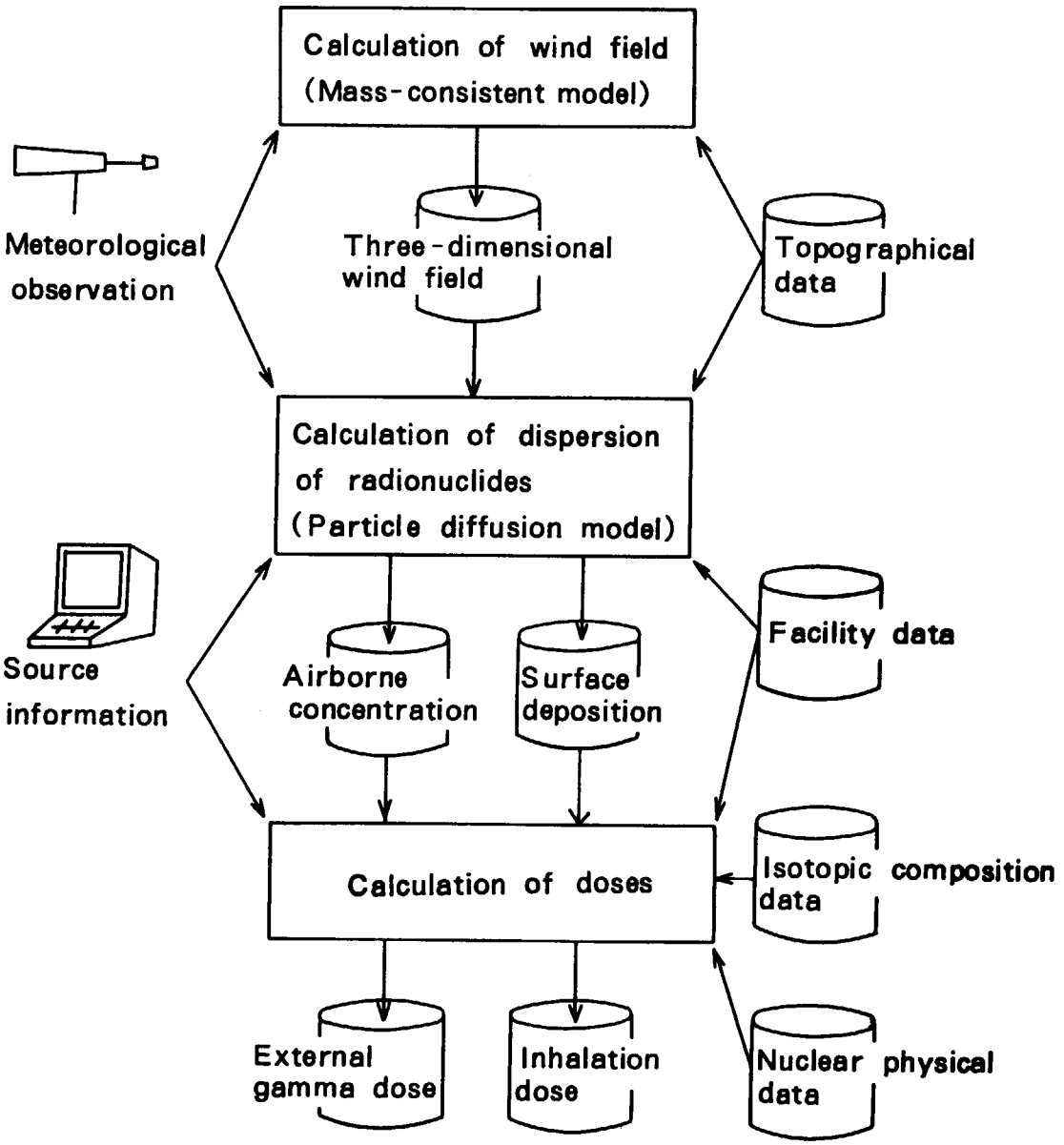

Fig. 3 Computational flow of WSPEEDI .

WSYNOP predicts three-dimensional(3-D) wind fields every 6 hours by using worldwide meteorological observed data or global meteorological forecast data provided from a meteorological agency, like ECMWF (European Center for Medium-range Weather Forecast). The usefulness of a mass-consistent model is apparent when observation data are used as input because otherwise a significant mass imbalance can be introduced during the interpolation of observed wind data onto 3-D grids. Moreover, when analyzed or forecast 3-D grid data are used as the input, a mass-consistent model serves to eliminate some mass imbalance which will be caused by the data conversion to WSPEEDI's coordinates and provides GEARN with terrain induced wind fields with a finer resolution.

GEARN predicts atmospheric transport, deposition onto the ground and radiological doses to the public using 3-D wind fields provided by WSYNOP, source term and geography. Although the models are basically the same as those of SPEEDI, several points have been improved for long-range transport under the experiences of Chernobyl simulations by SPEEDI[7], e.g., the coordinate system, consideration of variable air density and precipitation distribution, etc.

2.1 Coordinates and Grid System

In simulation of regional or hemispheric transport, the curvature of the earth should be considered. The straightforward way is to describe governing equations in the spherical coordinates. Another way is to project the 'spherical' computational domain onto a 'flat' computational space using a conformal map project. This way was adopted to define the coordinates in WSPEEDI. The horizontal coordinates are defined by

$$x=P_x(\theta,\phi),\quad y=P_y(\theta,\phi), \tag{1}$$

where θ and ϕ are the longitude and latitude, respectively. In this paper, the longitude is represented by θ instead of the conventional notation, λ, because λ is used to represent the Lagrange multiplier later. P_x and P_y are a pair of conformal projection functions such as the Lambert conformal projection or the polar stereographic projection. One of three conformal map projections is selectively used in WSPEEDI. These are Lambert Conformal Conic Projection (LCCP), Polar Stereographic Projection (PSP) and Mercator Projection (MP). The LCCP is suitable for regional scale simulations in the mid-latitudes. The PSP is used for hemispheric simulations. The MP is prepared for simulations in the equatorial region. Both LCCP and PSP can be used in the southern hemisphere. When a conformal projection is used, the true horizontal distance is transformed by the factor, m(x,y), referred to as the map scale factor, which depends on latitude only. The map scale factor is included in the formulation of models to cancel any distortion due to projection.

In the vertical direction, the models use a terrain-following coordinate (z* coordinate) defined by

$$z^* = \frac{z-z_g}{z_t-z_g} z_t = \frac{z-z_g}{h}, \left(h = \frac{z_t-z_g}{z_t} \right), \tag{2}$$

where $z_g(x,y)$ is the ground elevation and z_t the reference height. The reference height is set at 10 km, which is an approximate altitude of the tropopause. With the use of this vertical coordinate, the model topography becomes continuous and is greatly improved compared with the 'block topography' of SPEEDI which discretizes the continuous real topography.

A uniformly spaced computational grid is used horizontally, and, on the other hand, a variable

spacing grid is used vertically, in which the grid intervals gradually increase from 100 to 900 m upward.

2.2 Wind Field Model WSYNOP

WSYNOP, whose basic concept is the same as MATHEW developed by Sherman[10], has two successive procedures. The flowchart of WSYNOP is shown in **Fig. 4**. In the first step of the calculation, a wind field (u_0,v_0,w_0), called an 'initial guess', is estimated onto 3-D grids by interpolation and extrapolation of the observed or forecast wind data. In the second step, the 'initial

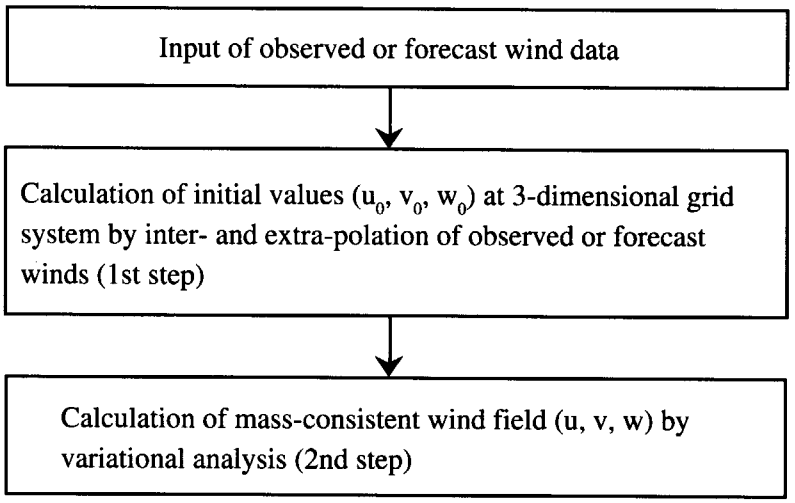

Fig. 4 Flowchart of a three-dimensional mass-consistent wind field model WSYNOP.

guess' is adjusted by a variational analysis so that the adjusted wind field $\mathbf{u} = (u,v,w)$ satisfies the mass continuity,

$$\mathrm{div}\,(\rho\,\mathbf{u}) = 0. \tag{3}$$

This problem is mathematically formulated as a variational problem to find (u,v,w) and λ which minimizes the functional,

$$E = \int \left[\alpha_1^2 (u-u_0)^2 + \alpha_1^2 (v-v_0)^2 + \alpha_2^2 (w-w_0)^2 + \lambda \cdot \mathrm{div}(\rho\,\mathbf{u})\right] dV, \tag{4}$$

where λ is the Lagrange multiplier, and α_1 and α_2 the weights which have positive values. The ratio of the weights α_1/α_2 prescribes the ratio between vertical and horizontal adjustment. If the ratio is well below one, the mass imbalance of initial guess is canceled mainly by the adjustment of the horizontal components. As the ratio becomes larger, the adjustment of vertical component becomes larger and the adjustment of horizontal components becomes smaller.

2.2.1 Estimation of initial guess

Worldwide meteorological data observed routinely by the member nations of WMO are exchanged among the nations by the Global Telecommunication System (GTS). The exchanged data include the surface and aerological wind data. Aerological observations are carried out at 0000 and

1200 GMT (Greenwich Mean Time) at the ten pressure levels from 1,000 to 100 hPa (hectoPascal (=mbar)). These data are used as the initial conditions for global meteorological forecast using a hydrodynamic numerical model in each country. The Japan Meteorological Agency provides users with observed data together with forecast data (called GPV: Grid Point Value) of the global, Asian and Japanese areas. The global forecast data are 30-hour forecasts on the horizontal grids of 5.0×2.5 degrees, dividing the global area, and on vertical grids at the surface and the same pressure levels as the observed. Therefore, two types of meteorological data, i.e., worldwide observed wind data and global forecast data in GPV, are expected as input for WSYNOP.

The initial guess is calculated by the following procedure:

(1) Preparation of tentative horizontal meshes, whose horizontal grid points coincide with those of WSYNOP and heights are at surface and the seven pressure levels of 850, 700, 500, 400, 300 and 250 hPa, which coincide with the observed levels,

(2) Horizontal interpolation of the wind data at the surface and pressure levels from 850 to 250 hPa onto the tentative horizontal meshes at the same levels, and

(3) Vertical interpolation of the horizontally interpolated winds onto the WSYNOP's grids located between the two levels of tentative horizontal meshes.

In the horizontal wind interpolation of observed data, the wind vector is determined using the proximate N observations with the weight of the inverse square of the distance between the grid and the observatory ($1/r^2_{obs,ij}$) as

$$(u_0, v_0)_{i,j} = \frac{\sum_{obs=1}^{N} (u, v)_{obs}/r^2_{obs.\,ij}}{\sum_{obs=1}^{N} (1/r^2_{obs.\,ij})} \tag{5}$$

In case where GPV wind data are inputted, the wind vectors on tentative meshes are estimated by the weighted interpolation of GPV data on four GPV grids surrounding the objective grid point.

The vertical interpolation is made under the following assumptions:

(l) The depth of the surface layer is 200 m and the wind speed increases with height within this layer according to the power law, and

(2) Above the surface layer, the horizontal wind at each grid level is interpolated by

$$u_0 = a \log z + b, \tag{6a}$$

$$v_0 = c \log z + d, \tag{6b}$$

$$w_0 = 0. \tag{6c}$$

2.2.2 Variational analysis

The model is formulated in the map coordinate defined as Eq.(1). "Coordinate vertical velocity", w*, induced by the transformation of coordinate from the Cartesian to the terrain-following, is related to (u,v,w) in the Cartesian as

$$w^* = \frac{1}{h}(w - S_x u - S_y u), \tag{7}$$

where,

$$S_x = m\,(z^* - z_t)\,\frac{\partial h}{\partial x}\ , \qquad S_y = m\,(z^* - z_t)\,\frac{\partial h}{\partial y} \tag{8}$$

are the gradient of a z*-surface, m(x,y) the map scale factor, which is the ratio of transformed distance on a conformal map projection to the true distance. Equation (3) is rewritten under the assumption of compressible continuity in the z* coordinate in the following way:

$$G = \frac{\partial \rho}{\partial t} + \frac{m^2}{h}\left[\frac{\partial}{\partial x}\left(\frac{\rho hu}{m}\right) + \frac{\partial}{\partial y}\left(\frac{\rho hv}{m}\right) + \frac{\partial(\rho hw^*)}{m^2\,\partial z^*}\right] = 0. \tag{9}$$

The G (kg/m^3/s) is referred to as mass divergence in this paper. In any derivation below, the wind components are considered as elements needing adjustment. The 3-D density fields ρ are estimated by interpolating meteorological data to the 3-D grids. The ρ is assumed to be precise and excluded from elements to be adjusted. This assumption is plausible, because the variability of air density is much smaller than that of the wind components. Let (u_0, v_0, w_0) and (u,v,w) be a "initial guess" and mass-consistent wind field, respectively. Then, the magnitude of the adjustment is measured as

$$I = \int [\,\alpha^2_u\,(u-u_0)^2 + \alpha^2_v\,(v-v_0)^2 + \alpha^2_w\,(w-w_0)^2\,]\,dV, \tag{10}$$

where α_i(i=u,v,w) are the weights. The purpose of variational analysis here is to find a (u,v,w) field capable of satisfying Eq. (9) and minimizing I. According to the variational theorem, this problem is equivalent to finding u, v, w, and λ, which minimize the functional J,

$$J = \int E\,dV = I + \int \lambda\,G\,dV, \tag{11}$$

where $E = I + \lambda\,G$ and $\lambda\,(x,y,z^*)$ is the Lagrange multiplier. With Eq.(7) and $dV = (h/m^2)dxdydz^*$, Eq.(11) is developed as

$$\begin{aligned} J(u, v, w^*, \lambda) = \int [\,&\alpha^2_u\,(u-u_0)^2 + \alpha^2_v\,(v-v_0)^2 \\ &+ \alpha^2_w\,(hw^* + S_x u + S_y v - w_0)^2 \\ &+ \lambda\,G(u, v, w^*)]\,\frac{h}{m^2}\,dxdydz^* \end{aligned} \tag{12}$$

To minimize J, the Euler-Lagrange equations for each f (f= u, v, w* and λ),

$$\frac{\partial E}{\partial f} - \frac{\partial}{\partial i}\,\frac{\partial E}{\partial(\partial f/\partial i)} = 0 \quad (i = x, y, z^*), \tag{13}$$

must be satisfied using the associated boundary conditions as

$$\oint \delta(f)\left[\frac{\partial E}{\partial(\partial f/\partial i)}\,n_i\right] dS = 0 \quad (i = x, y, z^*), \tag{14}$$

where δ (f) is the arbitrary first variation of f and n_i (i =x,y,z*) is the outward positive normal at the boundary in analytical space. The resulting Euler-Lagrange equations for u, v, w* can be rearranged as

$$\frac{u}{m} = \frac{\rho}{2\alpha^2_u}\,\frac{\partial \lambda}{\partial x} - \frac{\rho\,(z^* - z_t)}{2h\,\alpha^2_u}\,\frac{\partial h}{\partial x}\,\frac{\partial \lambda}{\partial z^*} + \frac{u_0}{m}\ , \tag{15a}$$

$$\frac{v}{m} = \frac{\rho}{2\alpha^2_v}\frac{\partial \lambda}{\partial y} - \frac{\rho\,(z^* - z_t)}{2h\,\alpha^2_v}\frac{\partial h}{\partial y}\frac{\partial \lambda}{\partial z^*} + \frac{v_0}{m}\,, \tag{15b}$$

$$\frac{w^*}{m^2} = \frac{\rho}{2h^2}\left[\frac{1}{m^2\alpha^2_w} + \frac{(z^* - z_t)^2}{\alpha^2_u}\left(\frac{\partial h}{\partial x}\right)^2 + \frac{(z^* - z_t)^2}{\alpha^2_v}\left(\frac{\partial h}{\partial y}\right)^2\right]\frac{\partial \lambda}{\partial z^*}$$
$$- \frac{\rho\,(z^* - z_t)}{2h\,\alpha^2_u}\frac{\partial h}{\partial x}\frac{\partial \lambda}{\partial x} - \frac{\rho\,(z^* - z_t)}{2h\,\alpha^2_v}\frac{\partial h}{\partial y}\frac{\partial \lambda}{\partial y} + \frac{w^*_0}{m^2}\,, \tag{15c}$$

after some calculations. The associated boundary conditions become

$$\lambda\ \delta\ (u) = 0 \quad \text{(at x boundaries)}, \tag{16a}$$

$$\lambda\ \delta\ (v) = 0 \quad \text{(at y boundaries)}, \tag{16b}$$

$$\lambda\ \delta\ (w^*) = 0 \quad \text{(at z* boundaries)}\,. \tag{16c}$$

The Euler-Lagrange equation for λ is identical to the above continuity equation (9) and the associated boundary condition is automatically satisfied. Substitution of Eqs. (15a)-(15c) into Eq.(9) yields an elliptic-type partial differential equation for λ, where G_0 is the mass imbalance of the initial wind field given by

$$\frac{\partial}{\partial x}\left[\frac{h\rho^2}{2\alpha^2_u}\frac{\partial \lambda}{\partial x} - \frac{\rho^2(z^* - z_t)}{2\alpha^2_u}\frac{\partial h}{\partial x}\frac{\partial \lambda}{\partial z^*}\right] + \frac{\partial}{\partial y}\left[\frac{h\rho^2}{2\alpha^2_v}\frac{\partial \lambda}{\partial y} - \frac{\rho^2(z^* - z_t)}{2\alpha^2_v}\frac{\partial h}{\partial y}\frac{\partial \lambda}{\partial z^*}\right]$$
$$+ \frac{\partial}{m^2\partial z^*}\left\{\frac{\rho^2}{2h}\left[\frac{1}{m^2\alpha^2_w} + \frac{(z^* - z_t)^2}{\alpha^2_u}\left(\frac{\partial h}{\partial x}\right)^2 + \frac{(z^* - z_t)^2}{\alpha^2_v}\left(\frac{\partial h}{\partial y}\right)^2\right]\frac{\partial \lambda}{\partial z^*}\right.$$
$$\left. - \frac{\rho^2(z^* - z_t)}{2\alpha^2_u}\frac{\partial h}{\partial x}\frac{\partial \lambda}{\partial x} - \frac{\rho^2(z^* - z_t)}{2\alpha^2_v}\frac{\partial h}{\partial y}\frac{\partial \lambda}{\partial y}\right\} = -\frac{G_0}{m^2}\,, \tag{17}$$

$$G_0 = \frac{\partial \rho}{\partial t} + \frac{m^2}{h}\left[\frac{\partial}{\partial x}\left(\frac{\rho h u_0}{m}\right) + \frac{\partial}{\partial y}\left(\frac{\rho h v_0}{m}\right) + \frac{\partial(\rho h w^*_0)}{m^2\partial z^*}\right]. \tag{18}$$

The boundary conditions, Eqs.(16a)-(16c), are interpreted as $\lambda = 0$ at the "flow through" boundaries or $\delta\,(w^*)=0$ at the ground surface; $\delta\,(w^*)=0$ means that w* has a fixed value at the boundary. Therefore, Eq.(15c) is assumed to be zero at the boundary. Under an assumption of $w_0^* = 0$ at $z^*= 0$, this boundary condition satisfies the impenetrability constraint at the bottom boundary. To obtain the mass-consistent wind field, Eq.(17) is first solved. Then, λ is substituted in Eqs.(15a)-(15c) to calculate the adjusted wind components. In the above formulation, the weights α_i in the minimization kernel are the key parameters controlling the model results. Some studies referred to the empirical values of the weights (e.g., Ishikawa [11], Kitada et al[12]). The weights were assumed to be spatial constants throughout the computational domain.

The finite difference form of Eq.(17) is solved iteratively. A 'multicolor' SOR (Successive Over Relaxation) method is currently used to vectorize the code, which is an extension of 'red-black' SOR by Moussiopoulous and Flassak[13]. In judging the convergence of the solution, the iteration is executed until the divergence of the wind field is reduced to the desired magnitude for every computational grid (for details see Ishikawa[8]).

2.3 Concentration and Dose Model GEARN

2.3.1 Modeling of atmospheric dispersion

Regarding the model GEARN, the atmospheric dispersion of radioactivity is modeled by following the trajectories of a large number of marker particles, discharged from a source and moving in the downwindward direction. The schematic diagram of dispersed particles can be seen in **Fig.5**.

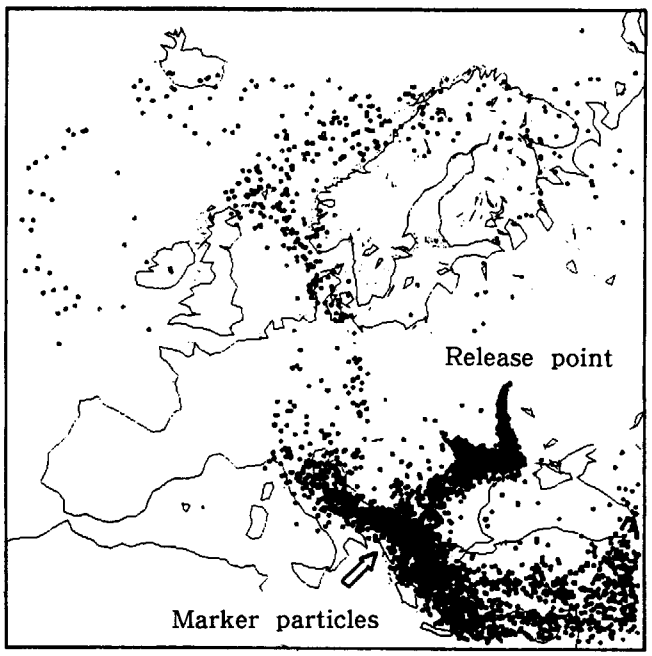

Fig. 5 Illustration of a particle random walk model GEARN.

The location of a particle for sequential time steps with time interval of Δt is determined from

$$x_{t+\Delta t} = x_t + m\,(u_p \Delta t + \delta x), \tag{19a}$$

$$y_{t+\Delta t} = y_t + m\,(v_p \Delta t + \delta y), \tag{19b}$$

$$z^*_{t+\Delta t} = z^*_t + w_p^* \Delta t + \delta z^*. \tag{19c}$$

In these equations, $(x,y,z^*)_t$ and $(x,y,z^*)_{t+\Delta t}$ are the positions of a particle at the start and end of the time step and m the map scale factor. The second term of the right-hand represents the transport of particle due to the airflow, and the third term the diffusion of particle due to air turbulence. As shown in **Fig.6**, the wind velocity (u_p,v_p,w_p^*) at the particle position can be calculated by the temporal and spatial

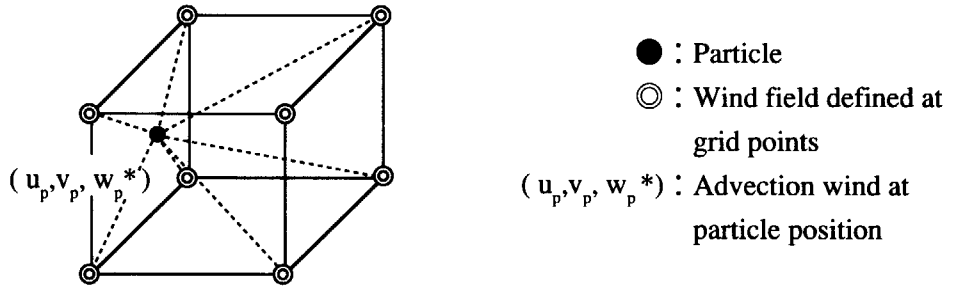

Fig. 6 Schematic diagram to explain the interpolation of wind vectors on the grids to the particle position.

interpolations of the wind vectors on the eight grid points, surrounding the particle. The equation for this is

$$(u, v, w^*) = \sum_{j=1}^{8} ((u, v, w^*)_j / r_j^2) / (1 / r_j^2) , \quad (20)$$

where $(u,v,w^*)_j$ are the temporally interpolated wind vectors at grid j and r_j the distance between particle and grid j. The wind field (u,v,w*) on the 3-D grid every 6 hours is provided from WSYNOP.

The diffusion terms δ x, δ y and δ z* are calculated based on a gradient-transfer theory. According to the theory, the diffusion term is shown as

$$\frac{\partial}{\partial i}\left(K_i \frac{\partial c}{\partial i}\right) = \frac{\partial K_i}{\partial i}\frac{\partial c}{\partial i} + K_i \frac{\partial^2 c}{\partial i^2} \quad (i=x, y, z^*) , \quad (21)$$

where K_i is the diffusion coefficient (m^2/s). The relation, $K_x = K_y$, is assumed, and they are represented by K_{hor}. The first term on the right-hand represents the transport of particles by quasi wind speed K_i', where $K_i' = \partial K_i/\partial i$, and the second term represents the random displacement whose standard deviation is defined by $\sqrt{2K_i\Delta t}$ with a mean of 0. Thus, the total diffusion displacement is expressed by the probability density function whose standard deviation is $\sqrt{2K_i\Delta t}$ whose mean equals $K_i'\Delta t$.

Since the model assumes the spatial constant of horizontal diffusion coefficient (i.e., $K_{hor}'=0$) in one step, the horizontal diffusion step is calculated by a simple distribution function whose mean is 0 and standard deviation σ_{hor} (m) follows by Gifford, applicable for long-range atmospheric transport,[14]

$$\sigma^2_{hor} = 2K_L t + \frac{v_0^2}{\beta^2}(1-e^{-\beta t}) + \frac{K_L}{\beta}(-3+4e^{-\beta t} - e^{-2\beta t}) , \quad (22)$$

where t is the travel time of a particle. According to Gifford, the values of the parameters, K_L(large-scale eddy diffusivity), v_0 (initial speed of a particle) and β (inverse of the time scale), are 10^4 m^2/s, 0.15 m/s and 10^{-4} s^{-1}, respectively. GEARN employs a uniform distribution function for the diffusion step and, for example, δ x can be shown as [15]

$$\delta x = [R]_{-\xi}^{+\xi} . \quad (23)$$

This equation shows the uniform random number within the range from $-\xi$ to ξ. To make the standard deviation of this distribution function equal to σ_{hor}, the value of ξ must be

$$\xi = \sqrt{6K_{hor}\Delta t} , \quad (24)$$

where

$$K_{hor} = \frac{1}{2}\frac{d\sigma^2_{hor}}{dt} . \quad (25)$$

Finally, by using uniform random number R(0) between 0 and 1, the horizontal diffusion can be rewritten as

$$\delta x = \sqrt{24K_{hor}\Delta t}\, R, \qquad \delta y = \sqrt{24K_{hor}\Delta t}\, R, \quad (R = 0.5 - R(0)) . \quad (26)$$

Regarding the vertical diffusion, the model considers the spatial distribution of the vertical diffusion coefficient. Therefore, as mentioned in Eq.(21), the vertical diffusion step is calculated based on the following standard deviation[16),(17)],

$$\begin{aligned}\sigma_z^* &= K'_{z^*}\Delta t \pm \sqrt{2(K_{0z^*} + \frac{1}{2}K'_{z^*}(K'_{z^*}\Delta t))\,\Delta t} \\ &= K'_{z^*}\Delta t \pm \sqrt{2K_{0z^*}\Delta t + (\Delta t K'_{z^*})^2},\end{aligned} \tag{27}$$

where K_{0z^*} is the diffusion coefficient at the particle position and K'_{z^*} the gradient of the diffusion coefficient. The distribution of diffusion coefficient K_{z^*} is simply defined as

$$K_{z^*} = \frac{K_z}{h^2} = \frac{1}{h^2}\frac{1}{2}\frac{dr}{dt}\frac{d\sigma_z^2}{dr} = \frac{1}{h^2}\,|u|\,\sigma_z\frac{d\sigma_z}{dr} \fallingdotseq \frac{1}{h^2}f_L|u|, \tag{28}$$

where $|u|$ is the absolute value of wind speed and f_L(L=1,2,3) is assigned to three layers, i.e., the atmospheric boundary layer, transition layer and the rest of troposphere, and the suffix, L, corresponds to the three layers. Here, the model assumes the top of atmospheric boundary layer is at a height of 900 m, followed by the transition layer with a depth of 100 m and the troposphere above 1,000 m above the ground. The values assumed here of f_1 and f_3 are 20.0 and 0.1, respectively. The value of f_1 for the atmospheric boundary layer corresponds to a slightly unstable condition, which can be acceptable if the elapsed time is at least 24 hours, in which the contaminants have experienced daytime vertical mixing. The value of f_3 is chosen so that the troposphere would always be stable. The value of f_2 is expressed as a linear function, connecting f_1 and f_3.

2.3.2 Air concentration

The concentration at each unit Eulerian cell C_{ijk} (Bq/m^3) is calculated by summing up the contribution of each particle to the cell with

$$C_{ijk} = \frac{1}{V_{ijk}}\Sigma b_{n,ijk}q_n. \tag{29}$$

Regarding this, suffixes i, j and k represent the cell number in the x- ,y- and z*-position, respectively. The q_n is the radioactivity (Bq) of the n-th particle. $b_{n,ijk}$ is the contribution ratio of the n-th particle to the objective Eulerian cell (ijk). This ratio is defined as the overlap ratio of a Lagrangian cell whose center is a particle position to the Eulerian model cell. V_{ijk}(=$h\Delta x\Delta y\Delta z^*/m_{ij}^2$) is the volume of the Eulerian model cell, where m_{ij} is the map scale factor.

2.3.3 Deposition

The dry deposition is calculated by the surface depression model. Each particle in the bottom layer with a width of Δz_d, provides a portion of its radioactivity to the surface. The decrease in radioactivity due to dry deposition is calculated as

$$-\frac{dq_n}{dt} = kv_g q_n, \tag{30}$$

where q_n is the radioactivity of the n-th particle, v_g the deposition velocity (m/s) and k (=$2(1-h_p/\Delta z_d)/\Delta z_d$) the weight which depends on the height of the particle, h_p. The deposition velocity depends on the type of nuclides and the condition of the surface[18)]. The deposition velocity of particulate ^{137}Cs is, for example, assumed to be 0.001 m/s, considering the range of the value based on reference[18)].

At the place where precipitation is observed, all the particles release a portion of their radioactivity to the surface below. The distribution of precipitation is estimated from observed data or

provided from GPV. The decrease in radioactivity due to the washout is calculated by

$$-\frac{dq_n}{dt} = \Lambda\, q_n, \tag{31}$$

where Λ is the washout coefficient (s^{-1}). The washout coefficients for elemental iodine and other particulates are functions of the rainfall intensity (mm/h) [19]. The model assumes that precipitation scavenging is caused only by the washout process. The total surface deposition at a horizontal location (i,j), DEP_{ij} (Bq/m^2), is calculated as

$$DEP_{ij}=\frac{1}{S_{ij}} \int \sum_n \left[\left(-\frac{dq_n}{dt}\right)_{dry} + \left(-\frac{dq_n}{dt}\right)_{wet}\right]_{ij} dt, \tag{32}$$

where S_{ij} ($=\Delta x \Delta y/m_{ij}^2$) is the area of the horizontal mesh. The summation in the integral is taken with respect to the particles existing inside the air column above surface area S_{ij}.

2.3.4 Radiological doses

In the model, the air dose rate, external γ dose and internal doses to inhalation are calculated. Air dose rate $D_{ij,air}$ (nGy/h) at 1.0 m above the ground surface is calculated by

$$D_{ij,\,air} = Df_{ex1} C_{ijo} + Df_{ex2} DEP_{ij}. \tag{33}$$

The first term on the right-hand shows the contribution from the airborne radioactivity calculated by a submersion model, where C_{ijo} is the surface air concentration and the coefficient $Df_{ex1}(E_\gamma)$ is taken from Poston et al.[20] with a proper unit conversion. The second term represents the ground-shine, in which the coefficient $Df_{ex2}(E_\gamma)$ is taken from Kocher et al[21]. External γ dose equivalent (Sv) is calculated from the time-integrated air dose rate.

Thyroid dose $D_{ij,thy}$ (Sv) due to iodine is obtained as

$$D_{ij,\,thy} = \int \frac{Df_{thy}}{0.693} \frac{\varepsilon\, T_e}{m} f_a\, R\, C_{ijo}\, dt, \tag{34}$$

where Df_{thy} is the conversion factor (g Sv/(MeV h)), ε the effective absorbed energy of iodine (MeV/dis), m the thyroid mass (g), T_e the effective half-life of iodine (h), f_a the thyroid uptake factor, R the respiratory rate (m^3/h) and C_{ij0} the air concentration of iodine at the human breathing level (Bq/m^3). The values of the parameters used in Eq.(34) are shown in **Table 1**, including data on the respiratory rate[22]-[24].

The internal dose $D_{ij,in}$ (Sv) due to the inhalation of other nuclides, e.g., ^{137}Cs, ^{90}Sr, etc., is

$$D_{ij,\,inh} = \int Df_{in}\, R\, C_{ijo}\, dt, \tag{35}$$

where Df_{in} is the dose conversion factor (Sv/Bq) shown in ICRP 30[25].

Table 1 Values of parameters used in Eq. (34).

Age group (nuclide)	fa	T_{eff} (day)	ε /m (MeV/g·dis.)	Respiration (m^3/day)
Infant (aged 1)	0.2			6
1-129		40	3.4×10^{-2}	
1-131		6.7	1.0×10^{-1}	
1-132		0.095	2.8×10^{-1}	
1-133		0.83	2.2×10^{-1}	
1-134		0.37	3.5×10^{-1}	
1-135		0.28	2.1×10^{-1}	
1-136		9.6×10^{-4}	1.0×10^{0}	
Child (aged 4)	0.2			14
1-129		40	1.7×10^{-2}	
1-131		6.7	5.0×10^{-2}	
1-132		0.095	1.4×10^{-1}	
1-133		0.83	1.1×10^{-1}	
1-134		0.37	1.8×10^{-1}	
1-135		0.28	1.1×10^{-1}	
1-136		9.6×10^{-4}	5.0×10^{-1}	
Adult (aged 20)	0.2			29
1-129		40	3.4×10^{-3}	
1-131		6.7	1.0×10^{-2}	
1-132		0.095	2.8×10^{-2}	
1-133		0.83	2.2×10^{-2}	
1-134		0.37	3.5×10^{-2}	
1-135		0.28	2.1×10^{-2}	
1-136		9.6×10^{-4}	1.0×10^{-1}	

*) fa ; thyroid uptake factor
T_{eff} ; effective half-life from thyroid

3. System Integration

3.1 Computer Network and Its Functions

The WSPEEDI is implemented on the computer network shown in **Fig.7**. The main computers in the network are two front-end workstations Λ 340 Σ, Fujitsu Ltd., Japan, for data communication and graphical output and two main-frame computers, M780 and VP2600, Fujitsu Ltd., both installed at the JAERI Computing and Information Systems Center. These computers are connected by a Local Area Network (LAN) at JAERI. The data communications workstation also has a line direct to the Japan Weather Association. For easy operation of computational codes in emergency situations, the WSPEEDI codes are systematized in combination with the system modules, e.g., the system control software, meteorological data processor, databases and graphic software. The primary functions of modules and computers are illustrated in **Fig.8**.

The global meteorological forecasts out to 30 hours are designed to be transmitted twice-daily from the Japan Meteorological Agency (JMA) via the Japan Weather Association (JWA) to the communications workstation having the meteorological data processor. The data are decoded, formatted and send to M780.

The M780 computer contains the system control software and databases including invariant data, e.g., worldwide geographical data, site data, etc. An operator initiates a WSPEEDI response using a time-sharing terminal connected to M780. The operations regarding data input, submission of jobs and displaying of the results are carried out through system control software based on the conversational mode. Release information is inputted in near real-time from a keyboard. When release information is not available in the early stage of the accident, the operator assumes the unit continuous release of mixed noble gases and iodines and starts the calculations. In this case, the results provide monitoring teams with relative air concentration and deposition distributions to determine the urgent monitoring areas. Furthermore, release rates of radionuclides can be estimated roughly by calculating the ratio of the measured to the calculated results. This estimation was actually attempted during the

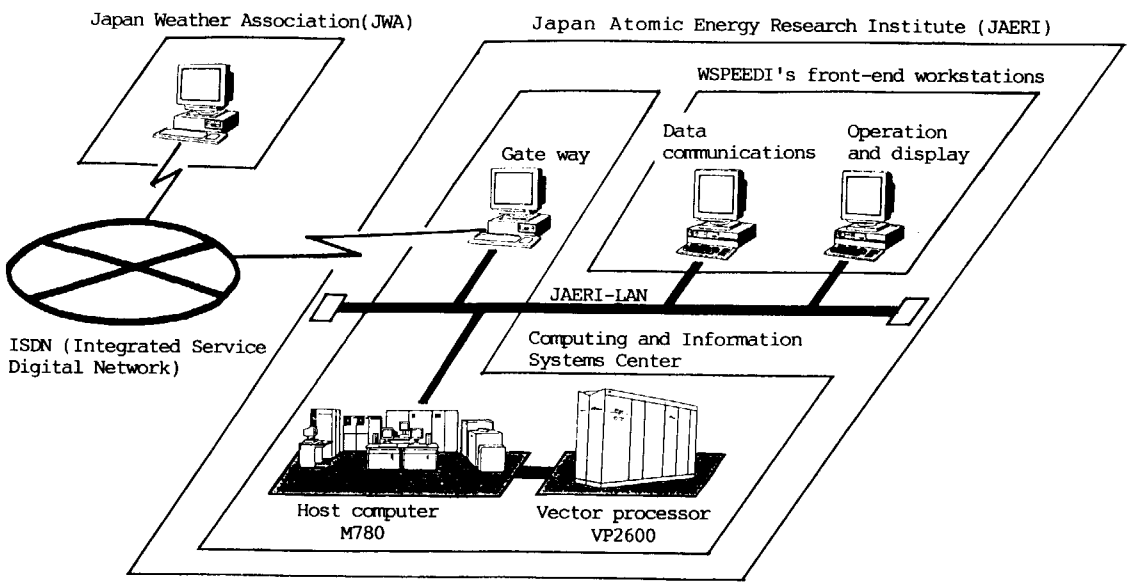

Fig. 7 The computer network of WSPEEDI.

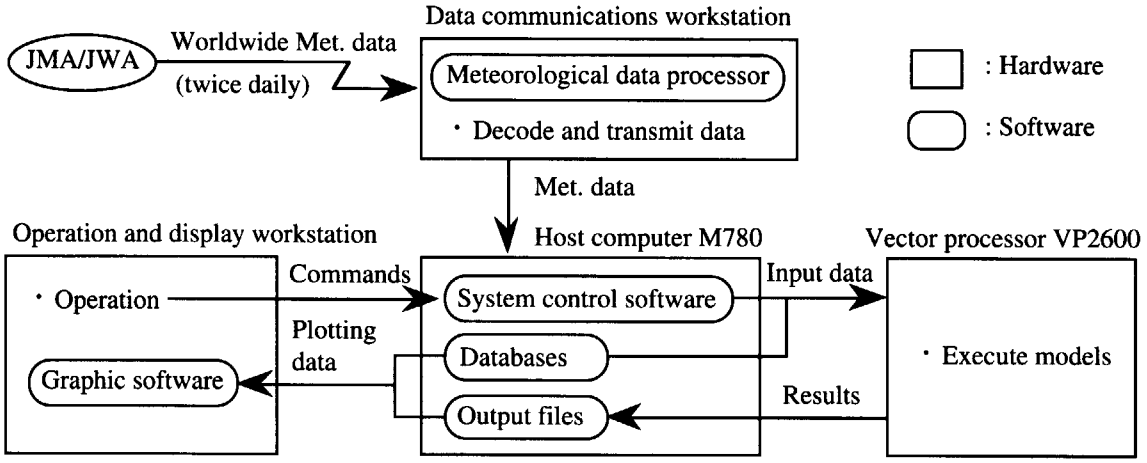

Fig. 8 The primary functions of modules and computers of WSPEEDI.

Chernobyl accident[7].

The operator usually performs forecasts twice-daily regarding the transport of radioactive materials out to 30 hours just after new GPV meteorological data are available. The calculations by WSYNOP/GEARN are carried out with a vector processor, VP2600. At the same time, near real-time data, e.g., source term and meteorological data, and data from the databases are also sent to VP2600. The computer programs of WSYNOP/GEARN are rewritten in a form suitable for vector processing. Furthermore, WSPEEDI receives special priority for responses in which the job leaves from the time-sharing management and can start without waiting time. The typical CPU time and memory size are shown in **Table 2**. This case, the CPU times for WSYNOP and GEARN are for calculating six 3-D wind fields and the transport of radioactive materials for three days, respectively.

The predicted results, e.g., wind fields, airborne concentrations, deposition, external γ doses and internal doses by inhalation are outputted into the files in M780 and then the operator can generate a variety of graphical outputs on the graphic workstation in the form of wind vectors or contours superimposed on a map.

Table 2 Typical CPU time and memory size.

Model	CPU time (s)	Memory size (KB)
WSYNOP	190	18,420
GEARN	91	14,270

3.2 System Control Software

The system control program based on the conversational mode is the nucleus of WSPEEDI. The control program receives and stores near real-time data, executes computations with physical models, and outputs and displays the calculated results. WSPEEDI is controlled by inputting commands through a operation workstation. The major commands of WSPEEDI are listed in **Table 3**. The SITE, TIME and REL commands are used for input of data such as the site location, release time, release

Table 3 The major commands to operate WSPEEDI.

Command Name	Explanation
EMER	Initiate or restart the code system
SITE	Set information of an accident site
REL	Set information of radioactive release
TIME	Set information of time parameter
WIND	Calculate the wind field of a specified region
CONC	Calculate the concentration of a specified region
GWIND, GCONC GDOSE	Display results over specified maps
SUB	Submit a computational module to the computer as a batch processing job
RUN	Process a computational module as a TSS job
GO	Same as the above
DPARAM	Display control parameters of SITE, REL, WIND, CONC, DOSE, GRAPH mode, or files
SET	Set control parameters of models
CLOG	Display the past convensational records logged in a logging file
HELP	Help users by displaying informations on commands
SAVE	Save the control informations for restart
END	End the session of the code system

When a 'Q' is added to each command, the system automatically questions the user about input parameters.

rate, etc. The WIND and CONC commands are used in calculating wind field, concentration and doses. The GWIND, GCONC and GDOSE commands are for graphic output of the calculated results of the wind field, concentration, deposition and doses, respectively.

The operator can easily initiate a WSPEEDI response with a choice of commands that generate the questionnaire to be displayed on a user-friendly menus, prompting the operator to input accident information such as time, location, and type of release and so on. The input data are unitary managed by the control software to avoid any conflicts between them. The input data given from the operator through the terminal are retained in the control program and they reflect the most recent values during the execution until other new input data are given to WSPEEDI.

The system is designed to be initiated with a minimum amount of external input data. For this purpose the control program automatically provides the physical models and system modules with standard data in the databases unless new values are inputted explicitly. For example, just by specifying site and facility name in the SITE command, data such as the location, topography of the objective region are automatically extracted from the databases and given to the models and modules.

Some examples of the menus in English are shown in **Fig.9 (a)** and **(b)**. The menus are largely self explanatory. **Figure 9(a)** shows a menu to input accident site. When an accident occurs at a site already registered in the database, the operator only has to input the site and facility name. Otherwise, the operator has to input the position of the release point in the latitude and longitude explicitly. **Figure 9(b)** shows a menu to submit a wind field calculation. Here, the model name, the calculation starting time, period, dump interval etc. are inputted. The parameters inputted in the previous operation are saved in a file and referred to as default values in the next operation. The default values are shown as character strings after the colons, and when they are changed, the values changed are assumed as the input.

```
INPUT NUCLEAR SITE DATA                                          ( a )

  INPUT TYPE  ==> __  (SELECT A OR B)

A) INPUT SITE NAME OF NUCLEAR ENERGY SITE
   (1)  SITE NAME       = _________
   (2)  FACILITY NAME   = _________
   (3)  RELEASE HEIGHT  = _________  (M)        (NUMBER OR *)
                                               (*:STACK HEIGHT IS USED)
    *   BURN UP         : _________  (MWD/MTU)

B) INPUT RELEASE POINT DIRECTLY
   (1)  LATITUDE             = ___ - ___ ' ___ "
   (2)  LONGITUDE            = ___ - ___ ' ___ "
   (3)  SITE TERRAIN HEIGHT  = _________ (M)
   (4)  RELEASE HEIGHT       = _________ (M)

   *    BURN-UP              :  _________(MWD/MTU)


PF1 : TIME MENU                          PF3 : CANCEL   PF4 : PREVIOUS MENU
PF2 : SUB. RETURN TO PRESENT MENU
NEXT MENU NAME ==> _______   (WHEN NOT SPECIFIED, GO TO GENERAL MENU)
```

```
--------------------------- W I N D ---------------------------
INPUT WIND FIELD CALUCLATION DATA AND SUBMIT                     ( b )

  (1)  WIND MODEL NAME = _________
  (2)  REGIONAL/LOCAL  = __          (SELECT  R OR L )

   *   STABILITY    : __
   *   EST. DATE    : ___ /___ /___
   *   EST. TIME    : ___ /___ /___
   *   EST. PERIOD  : ___ /___ /___
   *   DUMP. INT.   : ___ /___ /___

   F   WEATHER D.P. NAME : ____________________
   F   WIND    D.P. NAME : ____________________



EXECUTION MODE = __              ( 1:SET / 2:SUB )

PF1 : CONC MENU                          PF3 : CANCEL   PF4 : PREVIOUS MENU
PF2 : SUB. RETURN TO PRESENT MENU
NEXT MENU NAME ==> _______   (WHEN NOT SPECIFIED, GO TO GENERAL MENU)
```

Fig. 9 Some examples of user-interface menus to operate WSPEEDI;
(a) the menu to input accident site,
(b) the menu to submit wind field calculation.

3.3 Meteorological Data Processor

During the development of WSPEEDI, two types of meteorological data were considered as the input. One is surface and aerological 'observation' data from different countries, which are transmitted to JMA by WMO/GTS (World Meteorological Organization/Global Telecommunication System). Another possible meteorological source is the 3-D meteorological fields 'analyzed and forecast' by JMA based on worldwide observed data from WMO/GTS. In the first stage of the WSPEEDI develop-

ment, a meteorological data processor was constructed to input the worldwide observed data which had been already available via JWA. The processor checks the syntax of data in telegram form, decodes them, excludes any unreliable data, sorts the data with place and time and formats the values to a data file.

However, recently, 3-D analyzed and forecast meteorological data are available in Spring 1995 through JMA. Since meteorological observations in Asia are sparse and the meteorological forecast provides a time margin to take countermeasures, WSPEEDI newly uses the forecast results called GPV (Grid Point Values), from a general circulation model of JMA. The meteorological data obtained from GPV are listed in **Table 4**. Although GPV can provide forecasts over the globe, eastern Asia and Japan, WSPEEDI currently receives only global data. The global GPV data provides 30-hour forecasts of the wind component, temperature and precipitation on the grids with a horizontal spacing of 5.0×2.5 degrees regarding longitude and latitude and the vertical levels at the surface and then at the ten pressure levels from 1,000 to 100 hPa. Forecast wind data are available 0, 18, 24 and 30 hours from both 0000 and 1200 GMT (Greenwich Mean Time), where data at 0 hour mean the analyzed ones.

Prior to the formal open of the forecast data service by JMA, the construction and testing of the

Table 4 Meteorological data given from the GPV (global data).

Initialization time	Forecast time (h)	Resolution	P(hPa)	Content Z	U,V	T	RH	R
00, 12 GMT	00, 18, 24, 30	5°×2.5° (72×73)	sfc					○
			1000	○	○	○	○	
			850	○	○	○	○	
			700	○	○	○	○	
			500	○	○	○	○	
			400	○	○	○	○	
			300	○	○	○	○	
			250	○	○	○		
			200	○	○	○		
			150	○	○	○		
			100	○	○	○		

P : Pressure level, z : Height (m), U,V : wind speed (m/s), T : Temperature (°C),
RH : Relative humidity, R : Precipitation (mm/h)

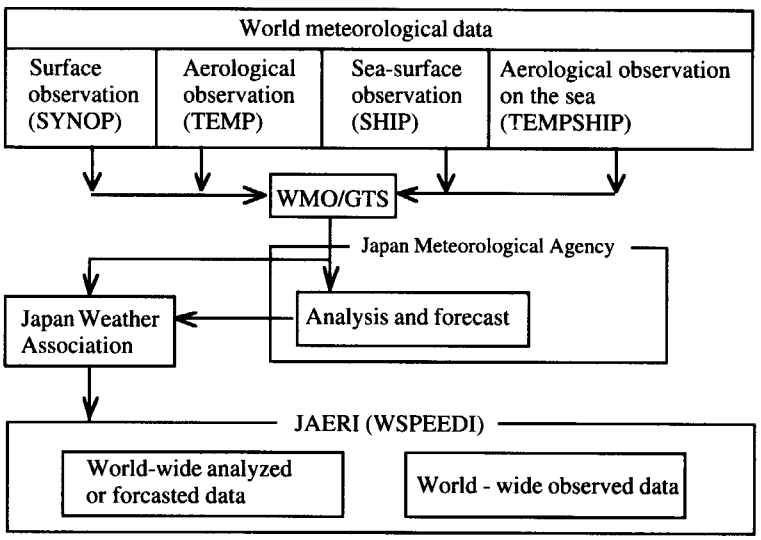

Fig. 10 Diagram of world meteorological data flow to WSPEEDI.

data communications line were carried out since October, 1994. **Figure 10** shows the meteorological data flow. JWA, whose computer system is connected to the JMA system, is one of agencies of JWA providing users with GPV data. The data line connecting the JWA computer system with the communications workstation of WSPEEDI is a high-speed digital line of NTT (Nippon Telephone and Telegram Co.) at 64 kbps. The global GPV data, consisting of 96 files, are transmitted by JWA twice daily to the WSPEEDI workstation. First dataset which comes at 0700 JST (Japanese Standard Time) contains the 30-hour forecasts whose initialization time is 1200 GMT(2100 JST) of the previous day. The second, coming at 1900 JST, gives the 30-hour forecasts initialized at 0000 GMT(0900 JST) of the same day. The communications workstation decodes the data and merges them into one file in the time sequential form. Furthermore, the unified file is automatically sent to the M780 computer and stored in the WSPEEDI meteorological file, which is maintained cyclically, that is, the last 12-day data are always kept and the oldest data are replaced by the newest when storage is full.

3.4 Databases

The system contains four databases which can be accessed by the numerical models and system modules which make use of the information for simulations, graphical output, etc. The databases and their contents are provided in **Table 5**.

Table 5 Databases and their contents.

Database	Content
Regional data	Topography, coast line, river, border
Site data	Site, plant, longitude, latitude, reactor type, stack height
Nuclear physical data	γ -energy, emmission rate, decay constant
Isotopic composition data	Isotopic rate of noble gases and iodines at shutdown

The worldwide geographical database contains topography, national borders, coastlines, major lakes and rivers. Worldwide topographical data are based on the U.S. Navy Global 10 Minute Elevation Data provided by the National Center of Atmospheric Research of the United States. It encompasses the entire globe with a 10'x10' resolution. Other geographical data were extracted from a commercial map database. The worldwide geographical data are stored on magnetic tapes as a master database. Since the area of concern will depend on the location and scale of the accident, WSPEEDI has a preprocessing function to extract the geographical data on the disk for the relevant region from the master database. Therefore, when operator needs to specify other areas, this function always precedes the start of WSPEEDI calculations. At present, WSPEEDI has the geographical data of three regions on a disk, e.g., the Asian, European and hemispheric regions, which are shown in **Fig.11 (a)**,

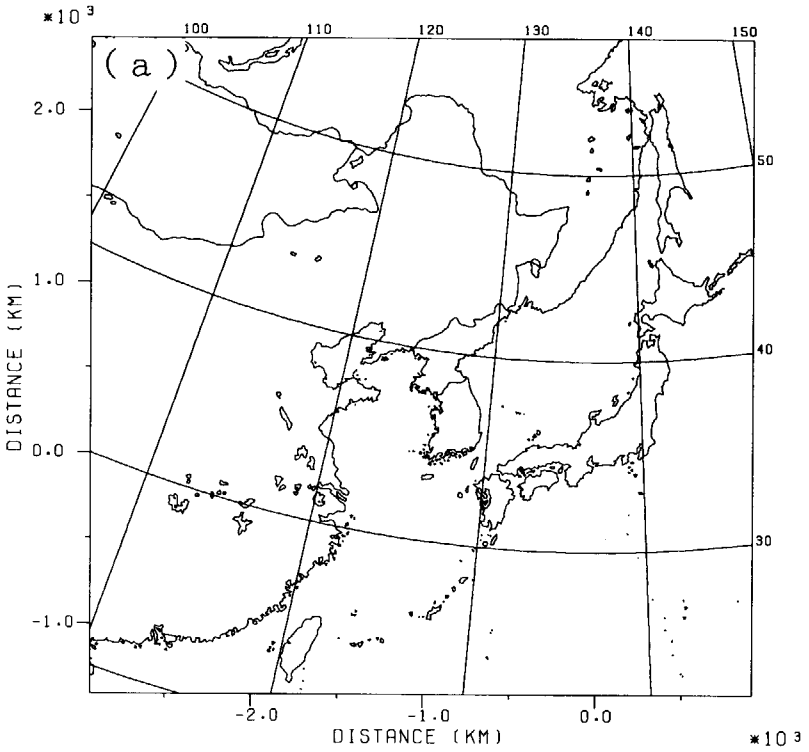

Fig.11 (a) Three geographical regions supported by WSPEEDI.
(a) The Asian region

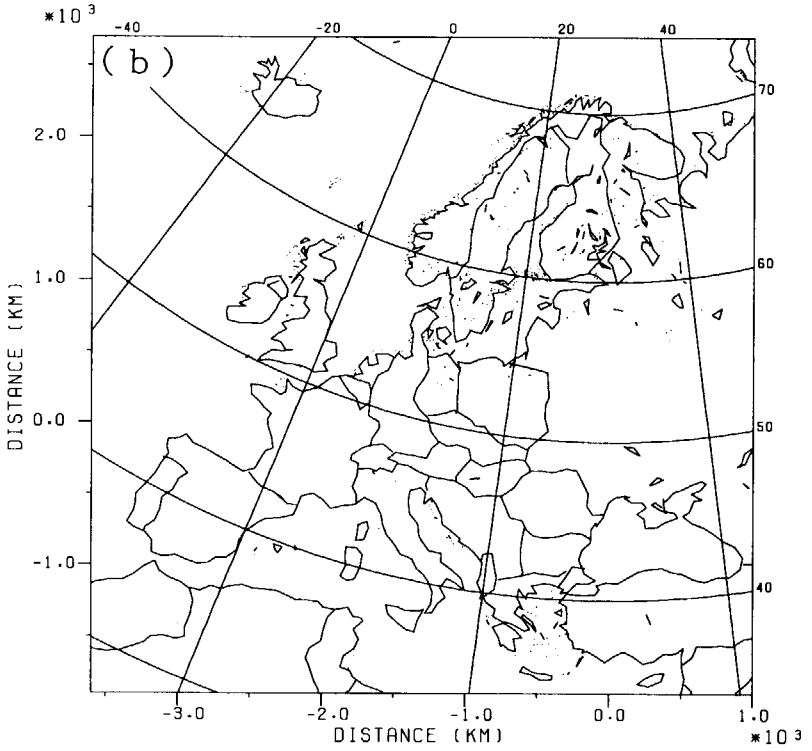

Fig.11 (b) Three geographical regions supported by WSPEEDI.
(b) The European region

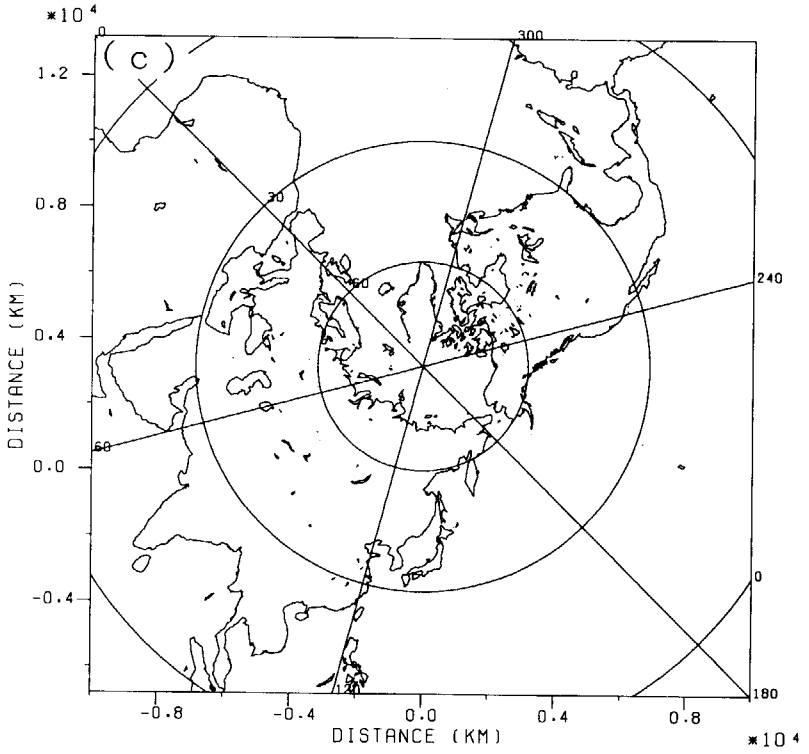

Fig.11 (c) Three geographical regions supported by WSPEEDI.
(c) The hemispheric region

(b) and **(c)**. These data are converted from latitude-longitude coordinates to map coordinates and rearranged onto 50×50 horizontal mesh of WSPEEDI. The number of mesh is decided to provide the results quickly during emergency, although it may be coarse for hemispheric simulations.

The site-data file contains the longitudes and latitudes, terrain heights, and types of objective power reactors. By specifying a site name and facility name in the input parameters of the SITE command, these data can be loaded from the file into the table in the system control program.

The physical constant data file contains decay constants, average photon energy, effective photon energy, each photon energy emitted from noble gases, seven isotopes of iodine, thirty-four isotopes of fission nuclides such as cesium and strontium, etc. The data are referred to dose calculations.

The isotopic composition data file contains an isotopic fraction of krypton, xenon and iodine in the fuel depending on the type of reactor and the burn-up. The data are used to estimate the isotopic composition in the initial stage of an accident.

3.5 Graphical Output

The graphic module of WSPEEDI produces a variety of plots using a map-oriented visual representation. The numerical and graphical outputs are shown in **Table 6**. Typical model results include 3-D wind fields, air concentrations of the materials, deposition on the ground, instantaneous and time integrated doses. The primary plots generated by the graphics are wind fields by arrow plots and contours of the air concentration, deposition and instantaneous and integrated doses using a geographical map overlay. The outputs include the legends that describe the release, unit and values of the contours, maximum point and time information.

Table 6 Numerical and graphical outputs.

	Numerical output	Graphical output
Wind field	U, V, W in (x, y, z, t) (m/s)	Horizontal and vertical wind field by arrow plots
Concentration	Airborne concentration in (x, y, z, t) (Bq/m^3)	Horizontal and vertical contour Temporal variation at arbitrary points
	Surface deposition in (x, y, t) (Bq/m^2)	Horizontal contour Temporal variation at arbitrary points
Dose	Air dose rate (nGy/h), external dose (mSv), inhalation dose (mSv) in (x, y, t)	Horizontal contour Temporal variation at arbitrary points

The graphic module is newly implemented on an engineering workstation running under the UNIX operating system, in addition to the traditional graphics which are directly controlled by M780. The numerical results computed by VP2600 are transmitted to the workstation through the LAN system. The workstation uses a high resolution color display for interactive input and output. Once the module is in operation, it is controlled mainly by using a point device (mouse) in conjunction with the menus (some limited keyboard operations are required for setting numerical values). The new graphical module has merits due to its easy operation, quick response and fine resolution.

Some examples of graphic output on the workstation are shown in **Fig.12(a), (b)** and **(c)**. **Figure 12(a)** shows a wind field near the surface over Europe at 1200 GMT, 23 October 1994 when European Tracer Experiment was carried out. The blue arrows on a 50×50 mesh show the regional wind field in which the arrows show the flow directions and their lengths correspond to the wind speeds. In the figure, an anti-clockwise circulation due to the low pressure can be seen over England. An example of the air concentration calculated in the Asian region is given in **Fig.12(b)**. In this case, the release point is on the east edge of the Asian continent and the material discharged flows toward Japan as a result of the westerly winds. Different color cells whose sizes are the same as the computational cell show the concentration distribution. The value of concentration which corresponds to each color is given on the right side of figure with the maximum concentration, unit, date and time. **Figure 12(c)** illustrates the surface deposition of ^{137}Cs discharged during the Chernobyl accident in which the distribution is represented in the same way as the air concentrations. This figure is a 3-day accumulated deposition after the beginning of the accident.

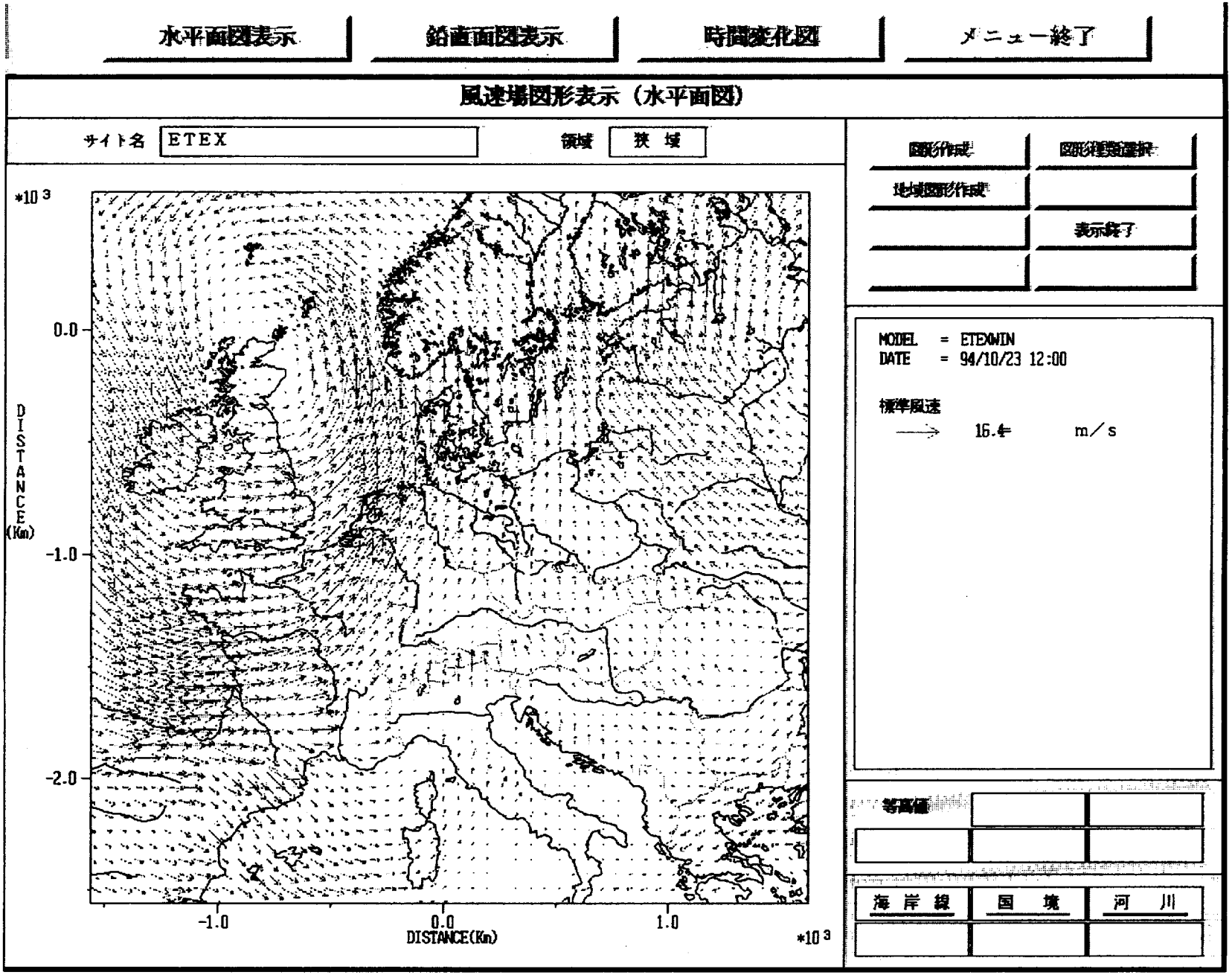

Fig.12 Some examples of new graphic outputs implemented in the workstation;
(a) wind field near the surface over Europe.

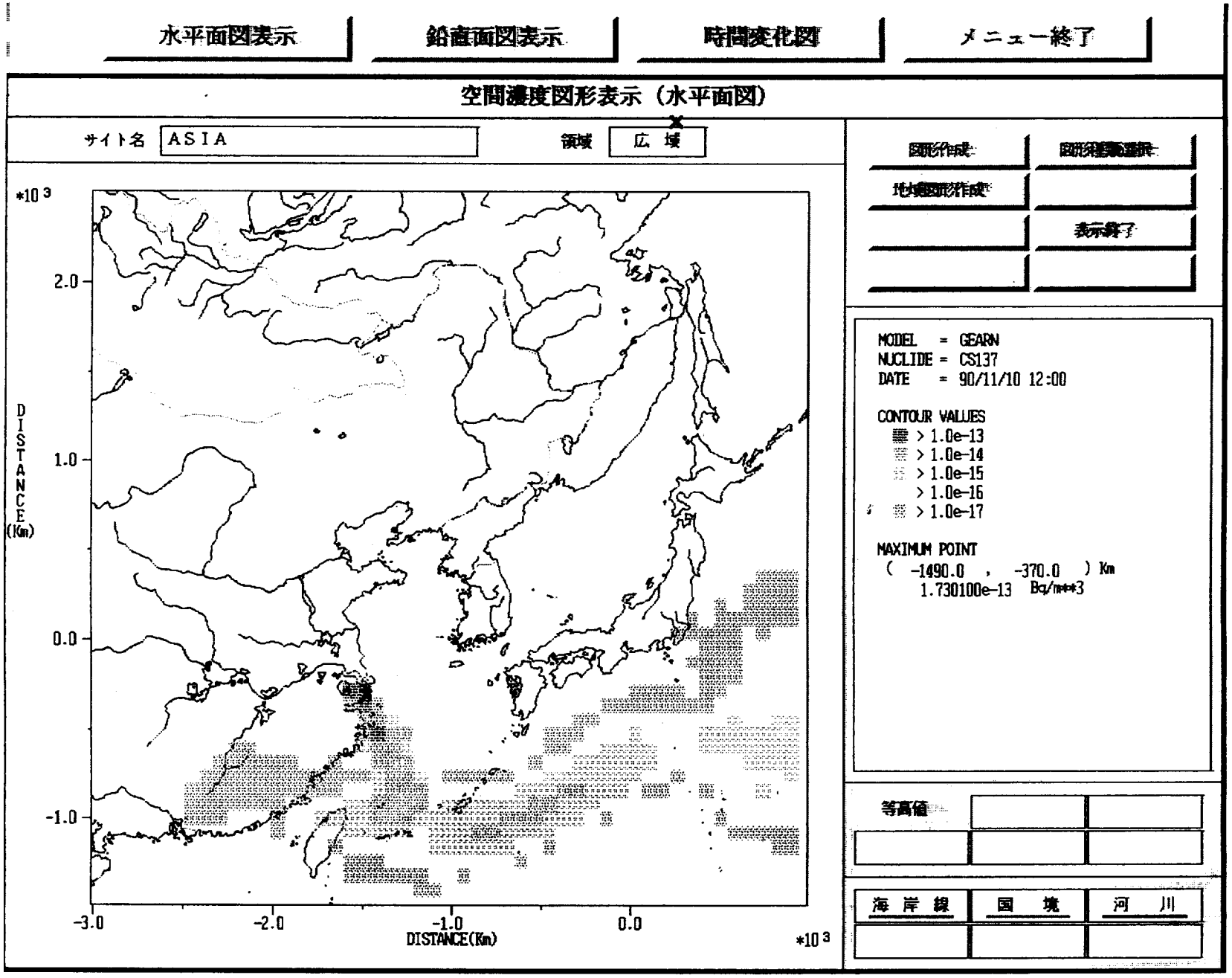

Fig.12 Continued.
(b) Air concentration calculated in the Asian region.

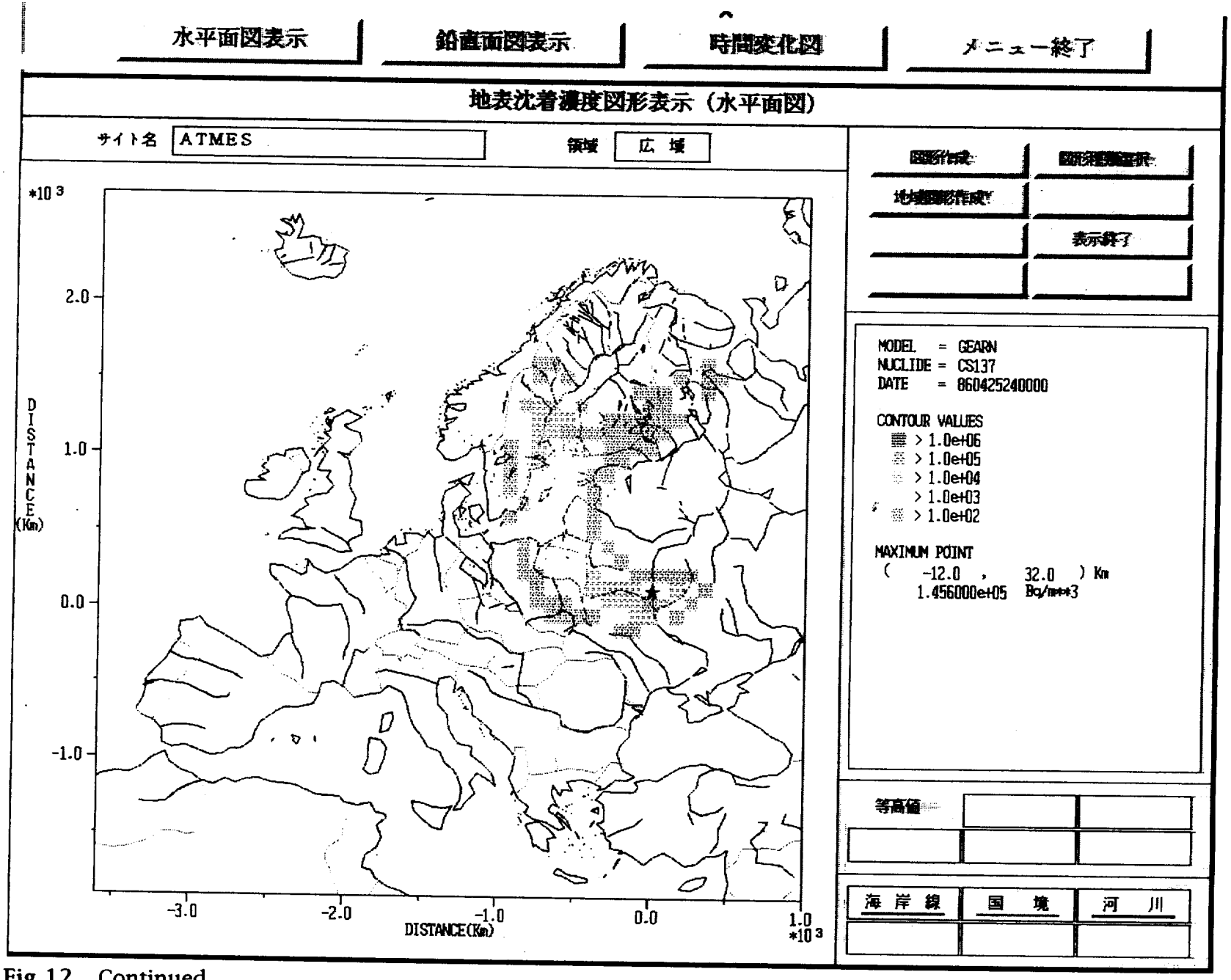

Fig.12 Continued.
(c) Surface deposition of ^{137}Cs during the Chernobyl accident.

4. Verification Studies

A variety of long range atmospheric transport models have been developed in different countries for application during emergencies, but their performance can only be estimated with much difficulty, because it is extremely hard for single institution to establish experimental databases for verification of long-range transport models. Moreover, it is almost impossible to conduct practical validation exercises using field tracer experiments taking into account the conditions of an accidental release, when the time constraints for near real-time response are important.

On these background, three international organizations, the Commission of the European Communities (CEC), the International Atomic Energy Agency (IAEA), and the World Meteorological Organization (WMO) sponsored two international model validation studies, called ATMES[6] (Atmospheric Transport Model Evaluation Study) and ETEX[26] (European Tracer Experiment). Regarding ATMES, performed during the period from 1986 to 1991, the Chernobyl accident data have been used retrospectively for model validations. Although ATMES was highly successful, the uncertainty associated with source term and monitoring procedures was also pointed out. Moreover, it was difficult to evaluate how well the models, used by ATMES participants, would respond to the near real-time predictions against an accidental release of radioactive materials. For these reasons, a follow-up international program ETEX has been agreed by the three ATMES sponsors, involving experimental studies of the long-range atmospheric transport over the European continent, to produce databases and to evaluate predictions capability. The experiments and related near real-time simulations by the models of the ETEX participants were conducted in Autumn 1994.

WSPEEDI was one of participants in both programs. This chapter describes the application of WSPEEDI to ATMES and ETEX. However, with regard to the simulation of the Chernobyl accident, the results recalculated based on the experiences of ATMES are shown. Thus, there are slight differences from the results of WSPEEDI in ATMES.

4.1 Simulation of the Chernobyl Accident

4.1.1 Framework of calculation

(1) Computational area

The transport of ^{137}Cs released from Chernobyl was simulated during the period from 2100 GMT (Greenwich Mean Time), 25 April to 0000 GMT, 11 May 1986. The computational area was 3,600 km by 3,600 km in the projected map, which is denoted by broken lines in **Fig.13** together with the distribution of the meteorological observatories. The vertical range was 3,000 m from the ground. The computational region was divided equally into $50 \times 50 \times 20$ cells, therefore the horizontal and vertical mesh intervals were 72 km and 150 m, respectively. Although consideration of the topography is one of the outstanding features of the WSPEEDI models, the topography was not included in this simulation; because the topographic data were not available when the analysis on the Chernobyl accident was carried out.

(2) Meteorological data

Since the analyzed and forecast data were not available from the JMA, the observed wind data at surface and at the pressure levels of 850 and 700 hPa were inputted to the wind field model WSYNOP. The distribution of surface and aerological observatories are shown in **Fig.13(a)** and **(b)**. Wind fields were calculated every 6 hours (0000, 0600, 1200 and 1800 GMT), which were inputted to the transport/diffusion model GEARN. In the GEARN, the wind field at the intermediate time, for instance at

(a) Surface observatories (b) Aerological observatories

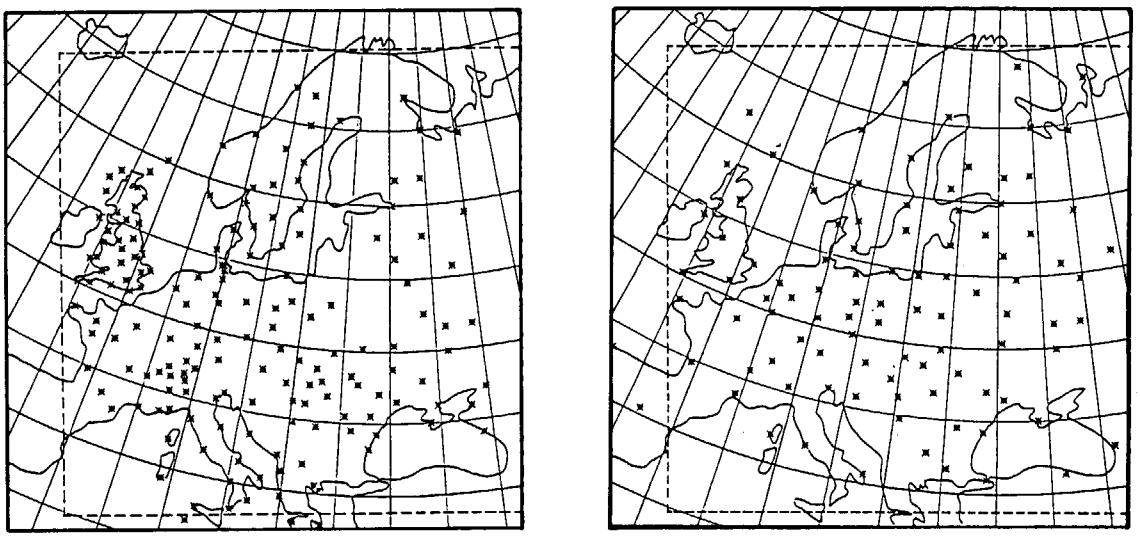

Fig. 13 The computational area for the Chernobyl simulation, which is denoted by broken lines together with the distribution of (a) surface and (b) aerological meteorological observatories.

O2 GMT, was interpolated from the 6-hourly wind field. The rainfall intensity was calculated from the precipitation data at the observatories in **Fig.13(a)**. Since the rainfall intensity should be given at every grid point, a simple interpolation technique was used. In this interpolation, the affection area of a single observatory was first calculated as a quotient obtained by dividing the total computational area by the number of observatories. Then, the precipitation at each grid point was defined by selecting the maximum precipitation value among these values at observatories whose affection area covered the grid.

(3) Source term

The source term was deduced from the former Soviet Union report to IAEA[27]. Although this report represented the release rate of each nuclide for the first day, the accumulated release amount of each nuclide until 6 May and the daily releases of the total nuclides from 27 April to 5 May, the daily release rate of each nuclide after second day was not shown. Therefore, the daily release rate of ^{137}Cs during these days were computed by multiplying the total daily release by the ratio of ^{137}Cs to the total nuclides on the first day (26 April). They are shown in **Fig.14**. The total of the computed daily ^{137}Cs release from 26 April to 5 May was 44 PBq (1.2 MCi), which was about 20 % greater than the reported total release of ^{137}Cs, 37 PBq (1.0 MCi). However, it is a reasonable estimation, because the estimation error of the original data was reported as 50 %[27]. The source term in the former Soviet report was estimated with reference to the local time at Chernobyl, which proceeds to GMT by 4 hours in summer. However, we neglected the time difference and used the daily release rate in **Fig.14** as the release rate from 0000 GMT to 2400 GMT for each day for computational convenience. Only for the initial release (first day), it was assumed that 11 PBq (0.3 MCi) of ^{137}Cs was released during 27 hours from 2100 GMT, 25 April to 0000 GMT, 27 April.

The radioactivity was blown up to the higher altitude at the initial stage of the accident because of explosions and fire. There were several estimates of the height of initial plume ranging from several hundreds of meters to about 2,000 m. Considering those estimates, we roughly assumed that the release height was 1,000 m during the first 9 hours of the accident and was 200 m after that.

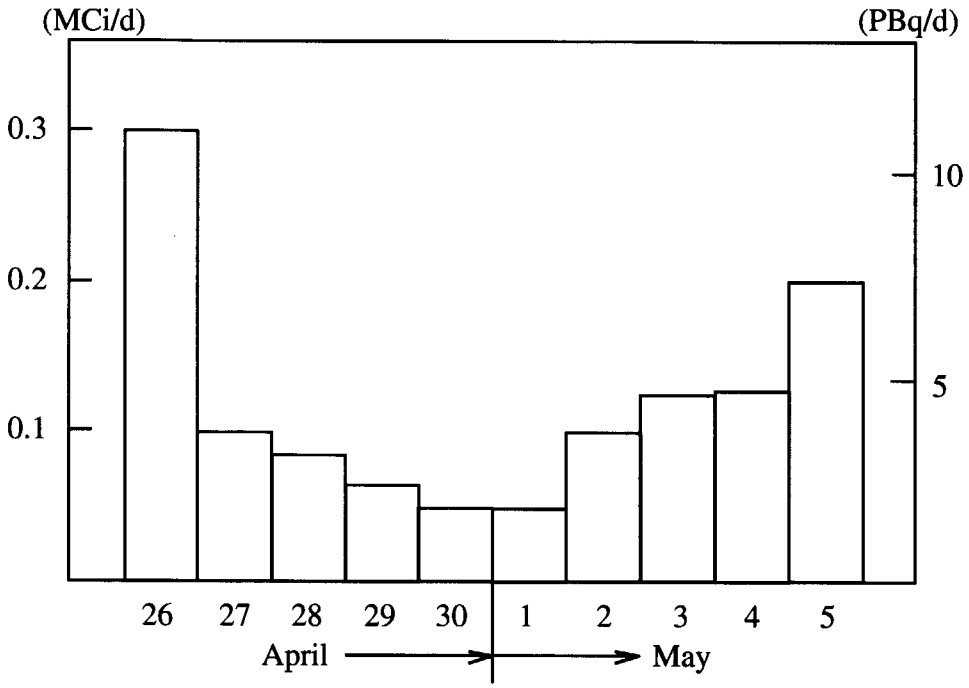

Fig. 14 The daily release rate of ^{137}Cs during the accident used for calculations.

(4) Diffusion condition

The depth of the mixing layer and strength of the diffusion are important parameters. The values of these parameters vary according to place. They also depend on local time. Typically, the diffusion is strong during the daytime because of the strong turbulence caused by insolation and it is weak during the nighttime. However, it is not easy to estimate the 3-D structure of these parameters from available meteorological data. Therefore, these parameters were assumed to be constant as described in Section 2.3.1.

4.1.2 Results and discussion

(1) Dispersion of ^{137}Cs over Europe

The evolution of surface air concentration is shown in **Fig.15**. The area where surface air concentration exceeds 3.7 mBq/m^3 is denoted by the lightly hatched area. The darkly hatched area represents where the surface air concentration exceeds 3.7 Bq/m^3. The arrivals of calculated plume at various European countries are compared with the data on the first observation date of Chernobyl radioactiv-

Table 7 Comparison of plume arrival date at several European countries.

Country	Salo[28]	Calculation	Country	Salo[28]	Calculation
Poland	Apr. 27	Apr. 26	Italy	Apr. 29	Apr. 30
Finland	Apr. 27	Apr. 27	FRG	Apr. 30	Apr. 29
Sweden	Apr. 27	Apr. 27	Switzerland	Apr. 30	Apr. 30
Denmark	Apr. 27	May 3	Turkey	Apr. 30	May 3
Norway	Apr. 29	Apr. 28	France	May 1	Apr. 30
GDR	Apr. 29	Apr. 29	UK	May 2	May 1
Hungary	Apr. 29	Apr. 29	Belguim	May 2	May 1
Austria	Apr. 29	Apr. 29	Netherland	May 2	May 1
Yugoslabia	Apr. 29	Apr. 30			

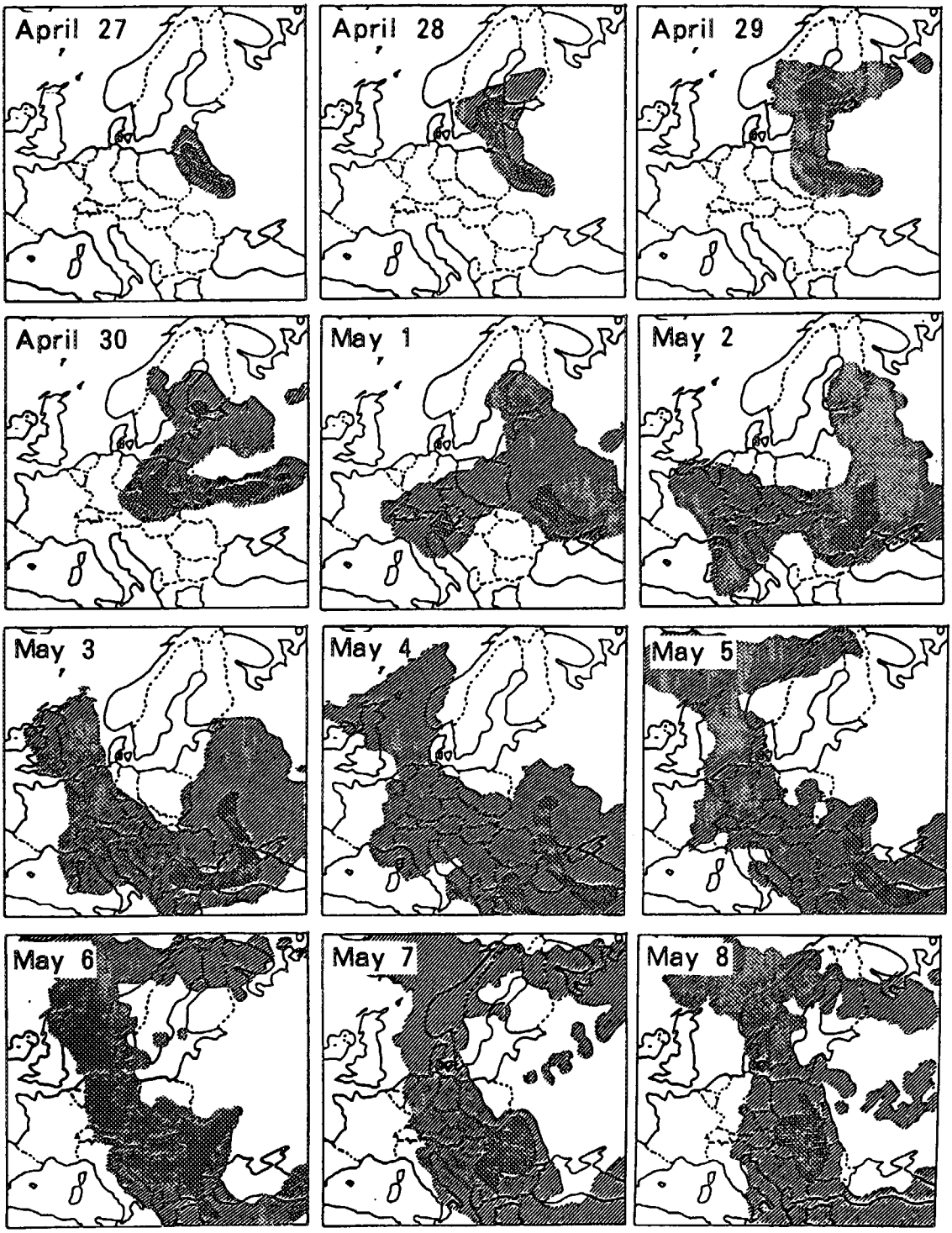

Fig. 15 The evolution of surface air concentration at 0000 GMT from 27 April to 8 May.

ity summarized by Salo[28] in **Table 7**. The calculated arrival date was defined as the date when the contour of 3.7 mBq/m^3 invaded a border of each country, because both the location and type of the measurement were not described by Salo[28].

In addition to the simulation results in **Fig.15**, in which continuous release for ten days were assumed, it also provided useful information to simulate the transport of ^{137}Cs discharged for each day independently. For example, the movements of the marker particles which represent ^{137}Cs released on

26 April and 4 May are shown in **Fig.16(a)** and **(b)**, respectively. These simulations revealed the following behavior of the cloud:

• The radioactivity released in the earlier hours of 26 April was transported to Scandinavian countries until the end of April.

• The radioactivity released during the period from the afternoon of 26 April to the morning of 27 April was transported to Central and Western Europe until 30 April. After that it was transported northward.

• The radioactivity released from the afternoon of 27 April to 3 May was transported to the east or south of Chernobyl, which covered Ukraine, Romania, Bulgaria, Yugoslavia, Greece and Turkey.

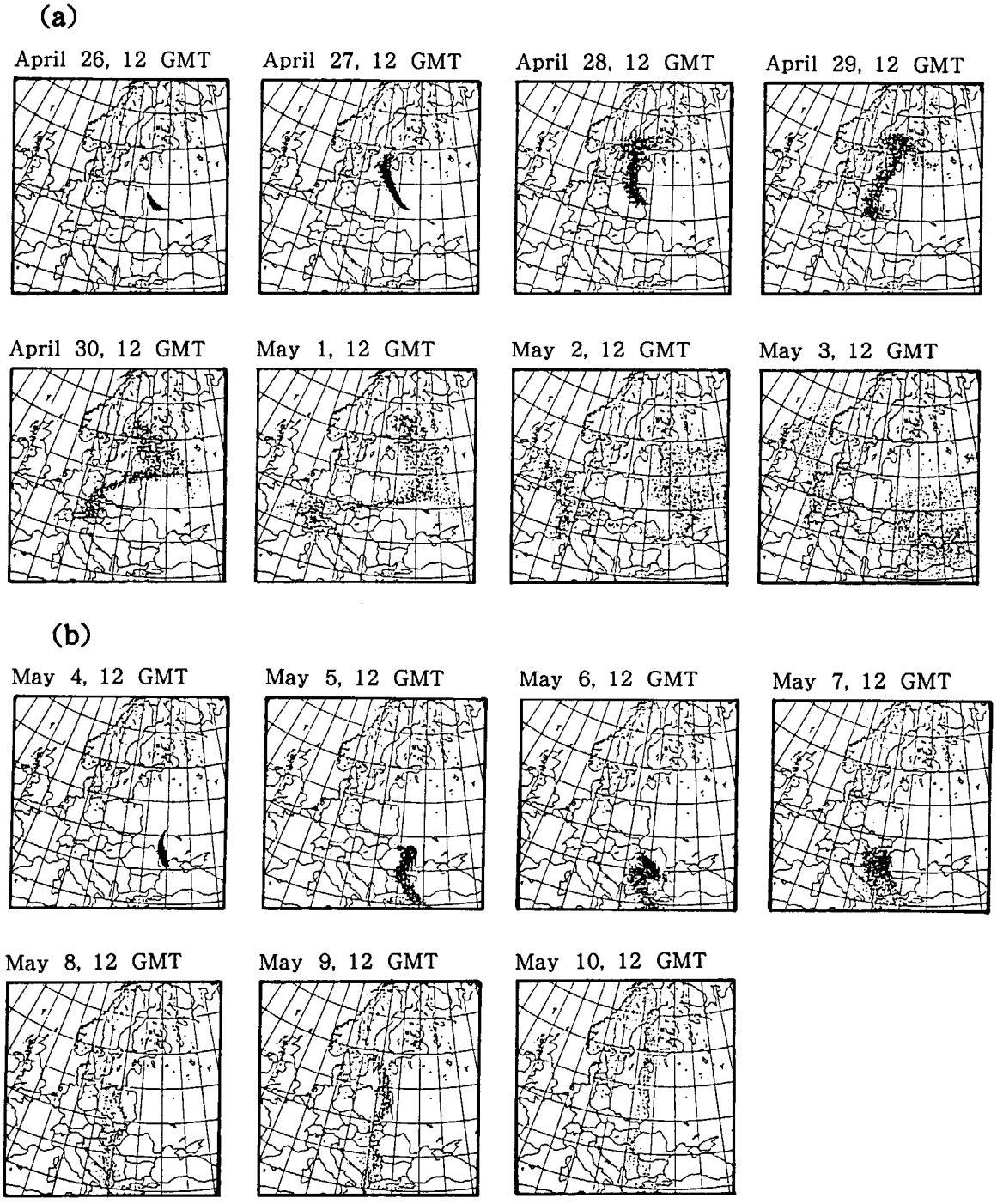

Fig. 16 Movements of marker particles which represent ^{137}Cs released on (a) 26 April and (b) 4 May.

• The radioactivity released on 4 and 5 May was first transported to the southwest of Chernobyl and was finally transported to the north, covering Central and Northern Europe as shown in **Fig.16(b)**.

(2) Comparison of surface air concentration

The calculated surface air concentrations are compared with measurements[29)-41)] in **Fig.17** at several locations. The solid line represents the calculated concentrations. The measurements are represented by the broken line and/or marks. The background value of the surface air concentration was 10^{-6} to 10^{-5} Bq/m^3 over Europe before the accident.

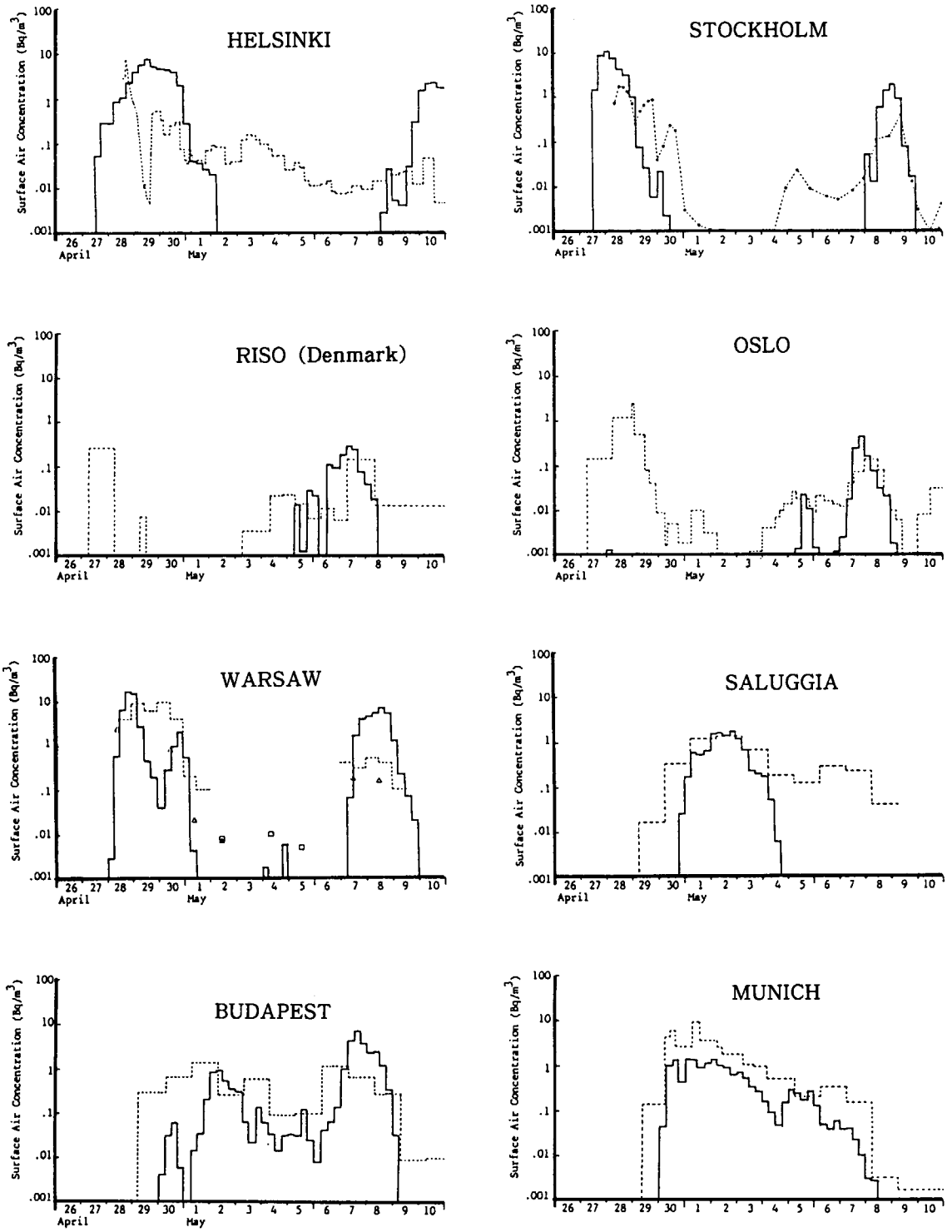

Fig. 17 Calculated surface air concentrations compared with measurements at several locations.

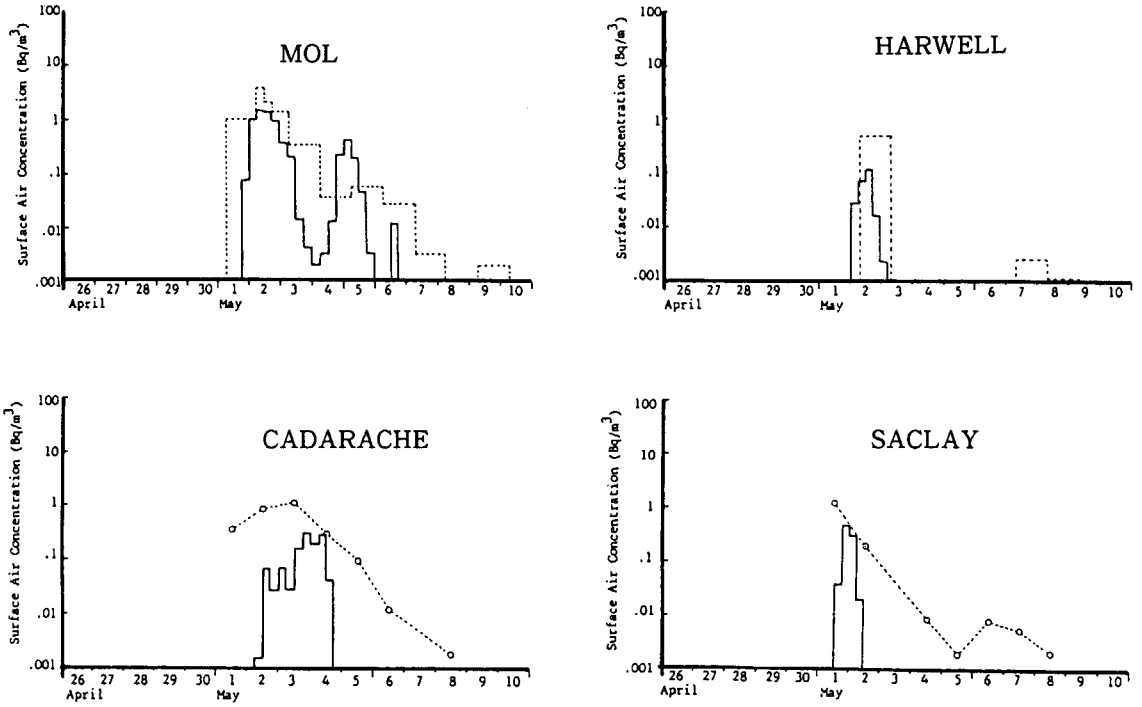

Fig. 17 Calculated surface air concentrations compared with measurements at several locations (continued).

At Stockholm, Warsaw, Budapest, Riso and Oslo, two major increases of radioactivity, one at the end of the April and the other in early May, were measured. Among these cities, the calculation simulated this feature at Stockholm, Warsaw and Budapest. As described in **Fig.16(a)** and **(b)**, the first increase was due to the emission on 26 and 27 April and the second increase was due to the emission on 4 and 5 May. At Riso and Oslo, however, the calculation did not simulate the increase in the air concentration at the end of April, although the second increase in May appeared. The exposure rate measured at Riso[42] showed that first arrival was around noon of 27 April. Seeing the calculated dispersion pattern in **Fig.15**, it seems that the calculation failed to simulate it.

The calculated air concentrations were in good agreement with the measured ones throughout the calculation at Munich. At Mol and Harwell, ^{137}Cs began to be found in the surface air after 1 or 2 May. The calculated concentration was in good agreement with these measured concentrations. The difference in the calculated and measured arrival time was within a half of a day. The difference in the magnitude of air concentration was within the order. These calculations suggested that the models simulated the transport of radioactivity to Western Europe quite well.

At Saluggia, Saclay and Cadarache the arrival of radioactivity was well simulated. However, the calculated concentration dropped abruptly after a few days, although significant concentrations were continuously measured after that. In a similar manner, at Helsinki the detection of radioactivity between 2 to 7 May is not explained by the calculation. The measured surface air concentration sometimes showed short-term variations as seen at Stockholm and Helsinki. However, the calculation did not follow these short-term variations. These variations in measurements were, presumably, associated with the local meteorology such as the development of a surface stable layer during night-time or land/sea breezes. The measurement of surface concentration is often affected by these local meteorology. The present models, WSYNOP/GEARN do not consider the local meteorology precisely, so that the calculation did not follow the short-term variations.

The correlation of the measured and calculated concentrations is shown in **Fig.18**. In this comparison, both measured and calculated results were reproduced to the daily averaged concentration with a consideration in the time of the filter change in the measurements. Totally, 125 points are plotted in **Fig.18**. For 51 points (40 %) the ratio of measured to calculated value was within a factor of 10. An agreement within a factor of 5 occurred in 33 points (26 %). However, there were 51 points on the vertical axis, which indicated that the calculated values were less than 10^{-4} Bq/m^3. In general, the agreement was good when the concentration was higher than 10^{-2} Bq/m^3, but it was worse when the measured concentration was lower. This suggested the possibility that the calculated cloud did not dispersed enough to explain the measured low concentrations. This is probably because the simulation tentatively extended the horizontal diffusion parameter used in a local-scale to the 2,000 km scale. However, based on this failure in **Fig.18**, a horizontal diffusion parameter shown in Eq.(22) was newly introduced and the results were improved (see detail Ishikawa[43]).

(3) Comparison of deposition

The accumulated surface deposition until 0000 GMT 11 May is shown in **Fig.19**. The characteristic feature was that there were many isolated areas having high values. These corresponded to the areas of precipitation. The calculated deposition accumulated until 10 May are compared with the measurements [31],[37]-[39],[44],[45] in **Table 8** at several locations. The calculated values were in good agreement with the measured ones at these locations, although the modeling of dry and wet deposition process has uncertainty. It is probably because the comparison of temporally accumulated deposition neglects the temporal discrepancy between the calculated and the measured results in some degree.

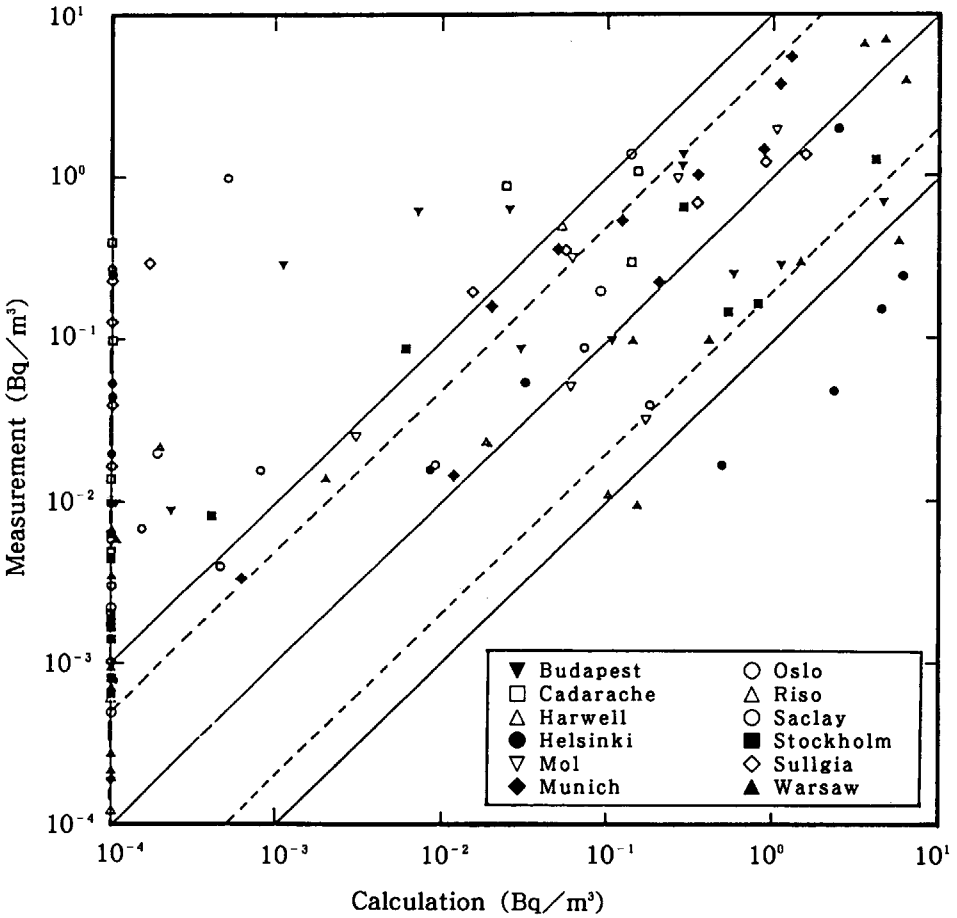

Fig. 18 Correlation of daily averaged surface air concentrations between the measured and the calculated.

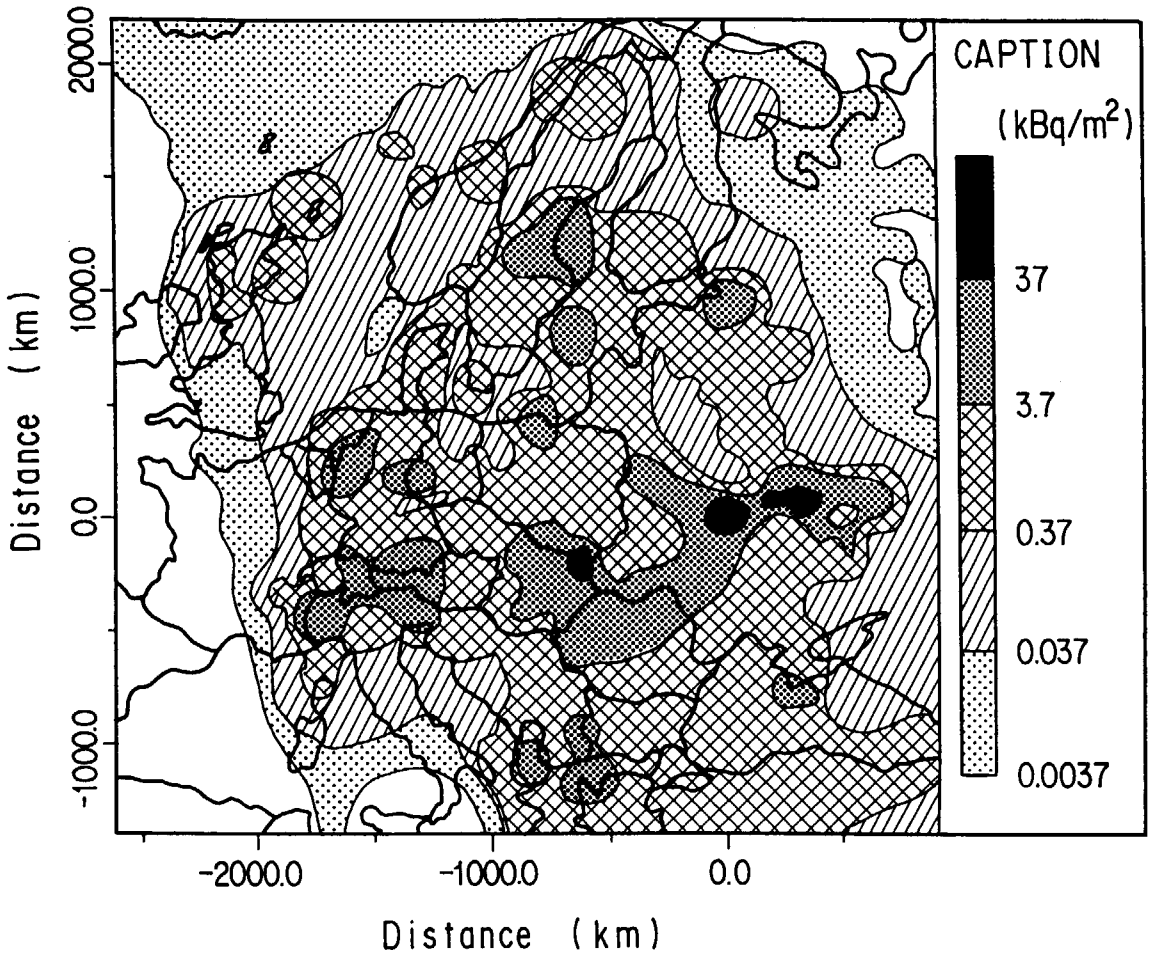

Fig. 19 Calculated deposition of ^{137}Cs accumulated until 0000 GMT, 11 May 1986.

Table 8 Comparison of calculated and measured surface deposition (kBq/m^2) accumulated until May 10.

Site	Calculation total (wet)	Measurement total (wet)	Major rainfall
Riso	0.644 (0.619)	- (0.672)	May 7 ~8
Munich	17.5 (17.2)	18.0 (-)	Apr. 29~30
Saluggia	18.2 (18.0)	17.5 (-)	May 2~4
Mol	1.63 (1.49)	- (1.98)	May 3~4
Helsinki	1.12 (0)	2.08 (-)	———
Budapest	4.32 (3.72)	5.59 (-)	May 1 and May 8~9

However, it should be noted that the calculation of deposition included several causes of uncertainty. The estimation of precipitation distribution was a major cause of this uncertainty. The spatial representativeness of precipitation data is generally poor, because the rainfall is a localized phenomenon. Therefore, the precipitation distribution that was interpolated from the data at the observatories in **Fig.13(a)** was not so reliable. In addition, the values of the washout coefficient and deposition velocity varies in a wide range according to the individual situation.

4.1.3 Summary

The dispersion of ^{137}Cs from Chernobyl was calculated by a combination of the models, WSYNOP/GEARN. The performance of the models was evaluated by comparing the calculated results with the measurements. The results are summarized as follows:

(l) The transport of radioactivity from Chernobyl over Europe was qualitatively explained by calculations except for some locations such as Denmark and Turkey.

(2) However, the short-term variations of measured surface air concentrations, which are affected by sub-grid scale and short term (within the interval of input of meteorological data) meteorological conditions, were not simulated by the calculation. Thus, it is desirable to examine the appropriate grid size and the interval to consider the meteorological variations, in future.

(3) The calculated accumulated deposition until 10 May corresponded well with the measurements at six cities.

The results suggest that the combination of WSYNOP/GEARN works well as a computer model for estimating the long-range transport of radioactivity. Although some important parameters such as release height, mixing layer height, stability condition and deposition parameters were roughly assumed, the calculated results showed good agreement with the measurements. Considering that these parameters can hardly be defined well in an emergency situation, the described model performance seems to be able to be used from a practical standpoint.

4.2 Real-time Operation for European Tracer Experiment

4.2.1 Outline of ETEX

According to the reference[26], the overall objectives of ETEX are:

• to conduct a long-range atmospheric tracer experiment involving controlled releases under well-defined conditions together with coordinate atmospheric sampling at distances up to some 2,000 km;

• to provide notification of the tracer releases to institutes responsible for producing rapid forecasts of atmospheric dispersion over long distances and to test the capability of these institutes to produce such forecasts in near real-time;

• to evaluate the validity of their forecasts in the light of the subsequent environmental measurements;

• to assemble a database of source term, meteorological and environmental data which will allow the evaluation of other present or future long-range atmospheric dispersion models.

ETEX thus consists of three activities:

• tracer release and analysis,

• near real-time response analysis and

• atmospheric model evaluation.

(1) Tracer release and analysis

The ETEX experiment was carried out twice, 23 to 26 Oct. (Run 1) and 14 to 17 Nov. (Run 2), 1994. An atmospheric tracer gas, perfluoromethlcyclohexane (PMCH), was released from appropriate locations in Western Europe. The gas has the necessary characteristics, i.e., environmentally safe, non-toxic, inert and analytically sensitive, and it was in fact used in Across North America Tracer Experiment, ANATEX[46].

The study area encompassed the European region between 4° W to 25° E and 44° N to 64° N approximately, which included about 200 synoptic stations where the tracer samplers were located (**Fig.20**).

The release point, Rennes, France at 48.04° N and 2.01° W, was selected such that the tracer cloud included the majority of European countries. The tracer releases continued for 12 hours at ground level. The source strengths were 7.9 g/s for Run 1 and 11.3 g/s for Run 2.

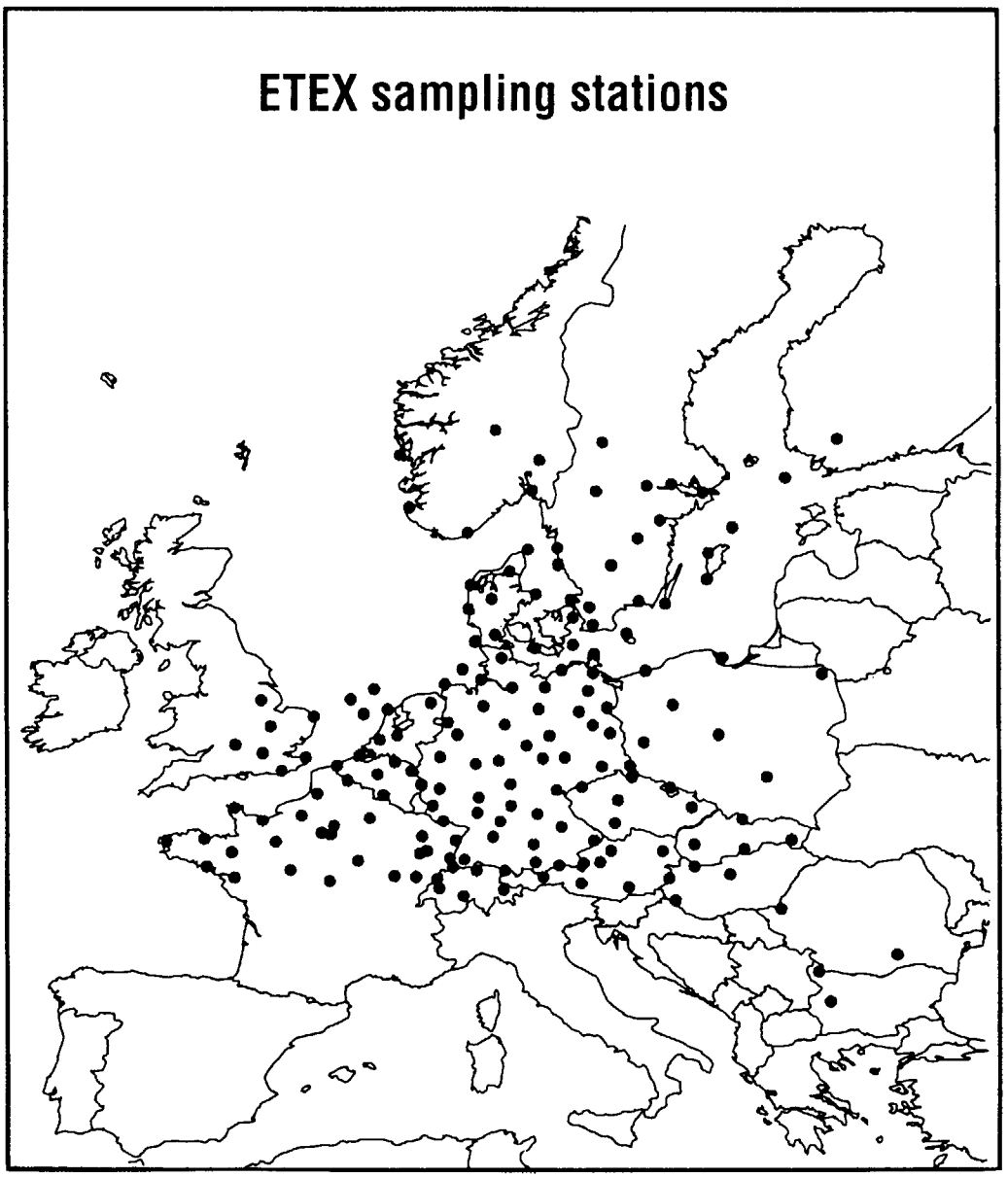

Fig. 20 Study area of ETEX, encompassed the European region between 4° W to 25° E and 44° N to 64° N approximately. Black circles show tracer samplers. (from Ref.(26))

Air samples were taken by a network of sampling stations located mainly at WMO synoptic meteorological stations in various countries. The samples were returned to the Joint Research Center of CEC (JRC-Ispra), Italy, where they were analyzed with analytical techniques based on gas chromatography developed at the Brookhaven National Laboratory.

(2) Real-time response analysis

Meteorological services and other institutes in various countries known to be involved in the long-range atmospheric dispersion emergency response, were officially informed about the proposed quick response test and formally invited to participate. Participants in the project, 25 institutions from 21 countries, were informed of the precise occurrence, location and characteristics of the release, e.g., the time and duration of release and exact source strength, only at the time of the release by facsimile and a computer mailing system(E-mail) via INTERNET, which is an international communications line. **Figure 21** shows the source information on Run 1 and Run 2 sent by facsimile from the ETEX

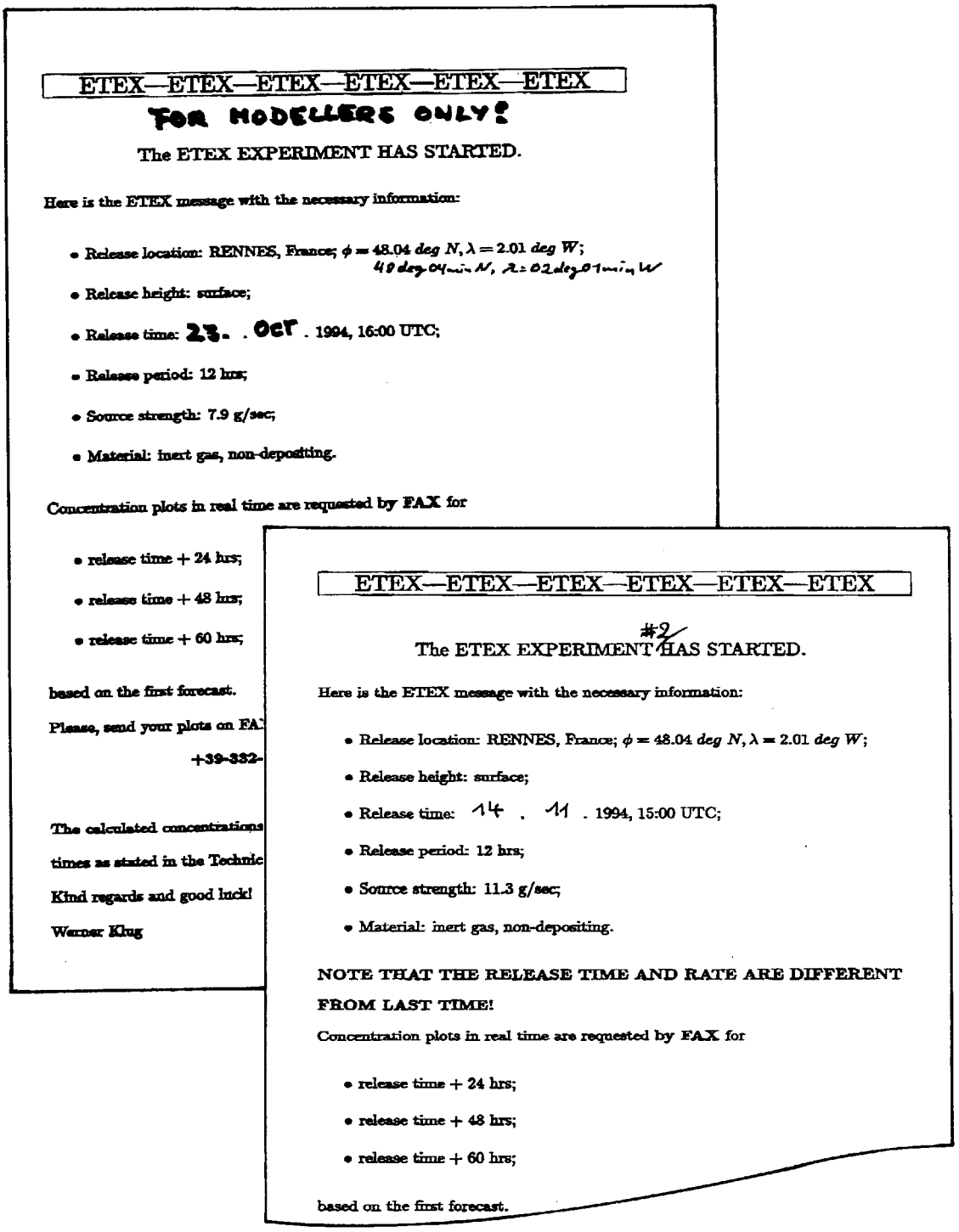

ETEX—ETEX—ETEX—ETEX—ETEX—ETEX

FOR MODELLERS ONLY!

The ETEX EXPERIMENT HAS STARTED.

Here is the ETEX message with the necessary information:

- Release location: RENNES, France; $\phi = 48.04$ *deg* $N, \lambda = 2.01$ *deg* W;
  48 deg 04 min N, λ = 02 deg 01 min W
- Release height: surface;
- Release time: 23. . Oct . 1994, 16:00 UTC;
- Release period: 12 hrs;
- Source strength: 7.9 g/sec;
- Material: inert gas, non-depositing.

Concentration plots in real time are requested by FAX for

- release time + 24 hrs;
- release time + 48 hrs;
- release time + 60 hrs;

based on the first forecast.

Please, send your plots on FA

+39-332-

The calculated concentrations

times as stated in the Technic

Kind regards and good luck!

Werner Klug

ETEX—ETEX—ETEX—ETEX—ETEX—ETEX

The ETEX EXPERIMENT #2 HAS STARTED.

Here is the ETEX message with the necessary information:

- Release location: RENNES, France; $\phi = 48.04$ *deg* $N, \lambda = 2.01$ *deg* W;
- Release height: surface;
- Release time: 14 . 11 . 1994, 15:00 UTC;
- Release period: 12 hrs;
- Source strength: 11.3 g/sec;
- Material: inert gas, non-depositing.

NOTE THAT THE RELEASE TIME AND RATE ARE DIFFERENT FROM LAST TIME!

Concentration plots in real time are requested by FAX for

- release time + 24 hrs;
- release time + 48 hrs;
- release time + 60 hrs;

based on the first forecast.

Fig. 21 The source information on Run 1 and Run 2 sent by facsimile from the ETEX evaluation team.

evaluation team. The task of the participants was to acquire the necessary meteorological information, calculate the cloud evolution for the next 60 hours, and transmit the predicted results as soon as possible to the ETEX evaluation team, located at JRC-Ispra.

Predictions transmitted had to cover the concentration distributions during the period of 60 hours from the beginning of the release (defined as T_0) and should consist of 3-hour average concentrations.

The participants could update their predictions every 12 hours when they could acquire new meteorological data. Therefore, five sets of predictions had to be performed at T_0, T_0+12h, T_0+24h, T_0+36h and T_0+48h. And, finally, the participants added an extra set (set 6) calculated using analyzed meteorological data for the whole 60 hours period. Only for the first set, the forecast evolution of the cloud at T_0+24, T_0+48 and T_0+60 hours were required to be sent in the form of contours of the air concentration on the map by facsimile within 6 hours after the notification of the release from the ETEX evaluation team. Other detailed predicted results of the 6 sets, which contained 3-hour averaged concentrations until T_0+60 hours, were sent within one month using diskette and the file transfer protocol (FTP) via INTERNET.

(3) Atmospheric model evaluation

Evaluation involves a comparison of the calculated and measured air concentrations at given locations. Therefore participants were required to produce concentration forecasts at a number of locations as well as concentration values on a mesh in latitude-longitude coordinates. The predictions are subsequently compared with the data from the experiment to allow the quality of the prediction to be judged. An analysis of the results obtained will include not only the differences between forecast and experimental data but also the timeliness of response, the behavior of communication lines and the quality of the emergency response system as a whole. An international discussion on the evaluation of the results from various institutions will start in Autumn, 1995.

4.2.2 Application of WSPEEDI to ETEX [47]

Topographical data and data communication lines for ETEX had been constructed since the formal invitation of WSPEEDI to participate in the ETEX project. The topographical database is shown in **Table 9**. It was made with a polar stereographic projection whose center was at 60° N and 10° E and covered a square of 3,175 km by 3,175 km. This region was divided into 50×50 grids with the width of 63.5 km. **Figure 22** shows the data communications flow. Communications on the notifica-

Table 9 Specification of topographical database used for ETEX.

Map projection	Polar stereographic projection
Origin of map	60° N, 10° E
Lower left corner	(-1555.5, -2560.65) km
Objective area	3175 3175 km
Cell number	50 50
Cell width	63.5 63.5 km

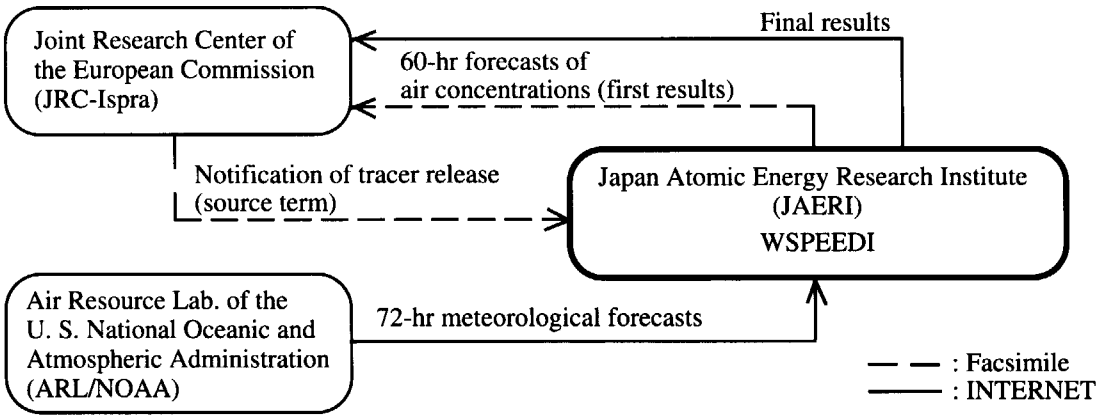

Fig. 22 The data communications flow used by WSPEEDI for ETEX.

tion of trace releases, return of forecast results, etc. were performed using facsimile, INTERNET and diskette. Although meteorological forecasts are formally expected to be provided from JMA, the 30-hour meteorological forecasts from JMA were insufficient to satisfy the 60-hour forecasts of air concentrations, which was the task given from the ETEX evaluation team. Therefore, for ETEX, 72-hour forecasts over Europe, which were specially available from ARL/NOAA (Air Resource Laboratory of the U.S. National Oceanic and Atmospheric Administration) during the ETEX project, were used. The data were defined on 65×65 grids on a map of the polar stereographic projection. The point (33,33) was the north pole and the width of grid was 381 km. Among these data, the 14×14 data which cover Europe were acquired twice daily using the FTP via INTERNET. The first dataset which comes at 0200 JST (Japanese Standard Time) contains 72-hour forecasts whose initialization time is 1200 GMT(2100 JST) of the previous day. The second, coming at 1400 JST, gives the 72-hour forecasts initialized at 0000 GMT(0900 JST) of the same day. Both include meteorological changes of every 6 hours. Hereafter, a set of meteorological forecasts is recognized by initialization time DD_HH, where DD is the date and HH the hour, e.g., the data 23_00 means 72-hour forecasts initialized at 00 GMT, 23. The communications workstation decoded these data and extracted the 9×9 data on the ETEX area. Finally, the data were sent to the M780 computer and stored in the WSPEEDI meteorological file. The data acquisition from ARL/NOAA and the data transmission from the WSPEEDI data communications workstation to M780 were made using FTP by manual. These operations were carried out within 5 minutes. Forecasts of the evolution of the tracer gas were carried out using WSPEEDI. Here, although the forecasts from ARL/NOAA already included 3-D wind fields, WSYNOP had the roles to eliminate the mass imbalance caused by the conversion of the NOAA data to the WSPEEDI computational grids and to provide GEARN with wind fields reflecting the terrain effect with finer resolution.

(1) Real-time response for Run 1

The progress with time of near real-time responses on Run 1 is given in **Table 10**. The date and

Table 10 The progress with time of near real-time response on Run 1.

Date	Time (JST)	
22 Oct.	18 : 36	Pre-alert to inform the possibility of the tracer release within 32 hrs.
23 Oct.	14 : 00	Acquisition of the forecast data 23_00 and pre-calculation of wind field.
24 Oct.	02 : 05	Notification to inform the source term. Start of the air concentration calculation using the wind field based on the forecast data 23_00.
	02 : 15	Acquisition of the forecast data 23_12. Contour plots of air concentrations based on the forecast data 23_00.
	03 : 15	Start of the wind field calculation using the forecast data 23_12.
	03 : 56	Start of the air concentration calculation using the wind field based on the forecast data 23_12.
	04 : 18	Contour plots of wind fields and air concentrations based on the forecast data 23_12.
	04 : 45	Transmission of the predicted results to the ETEX evaluation team.
	14 : 27	Acquisition of the forecast data 24_00 and start of the second prediction.
	15 : 23	End of the second prediction.
25-26 Oct.		The third to sixth predictions.
27 Oct.		Transmission of all the predicted results to the ETEX evaluation team by INTERNET.

time shown are Japanese Standard Time (JST). Pre-alert information which let the participants know the possibility of a tracer release within 32 hours reached at 18:36, 22 Oct. by facsimile and E-mail. The operation of WSPEEDI started from 23 Oct. The acquisition of the forecast data 23_00 started at 14:00, followed by the wind field calculations by WSYNOP started in the afternoon of 23 Oct. After that, we were ready to receive a notification on the tracer release. The notification shown in **Fig.21** reached at 02:05, 24 Oct. This notification gave the release point in longitude and latitude, time of the release and its duration, release height and source strength. These data were inputted through the commands to operate WSPEEDI. Although the wind field calculation based on the forecast data 23_00 had already ended beforehand, it was the just time to be able to acquire the new forecast data 23_12. Thus, we started the operation to get the new data in parallel with the prediction of the tracer gas dispersion and the plotting of the contours of the air concentrations based on the data 23_00. This work needed one hour, from 2:15 to 3:15. The wind field calculations using new data 23_12 were successively started at 3:15. The calculations are designed to be performed in a vector processor, VP2600. However, VP2600 had several large jobs needing huge memory over the weekend. Thus, the calculations for the first set were carried out on M780. Consequently, 40 minutes of CPU time was needed to finish the calculation although it normally takes only 3 minutes. We made a concentration calculation during the period from 03:56 to 04:10 and, subsequently, plotted nine figures, e.g., six wind fields every 12 hours for three days and the contours of air concentrations at T_0+24, T_0+48 and T_0+60. Finally the results requested were sent to the ETEX evaluation team in JRC-ISPRA by facsimile at 04:45 after examining the results.

The response for the second set started at 14:27, 24 Oct. to obtain new forecast data 24_00 from ARL/NOAA, after taking a rest. The calculations were carried out by using VP2600, which was available at that time. All the predictions for Set 2 ended at 15:23, which means the whole operation was completed within one hour. The CPU times for WSYNOP and GEARN were 158 sec. and 91 sec. on the VP2600 computer, respectively. However, the elapsed times from the submission to output were 15 and 11 minutes, because of the time sharing management in the CPU. The predictions continued twice daily until 26 Oct. to improve the results by using the last 72-hour forecasts from ARL/NOAA. The start time of the wind field calculations was slide 12 hours forward in the sequence so that the wind field based on the forecasts were replaced by the analyzed wind field, and finally, the wind fields based on diagnostic analysis of observed data only remained. The 6 sets of predicted results were sent by a diskette and FTP via INTERNET at 26 Oct.

The results of Set 1, which were based on the forecast data 23_12, are shown in **Fig. 23(a)-(f)**. The left, (a)-(c), are the predicted wind fields near the surface at 1200 GMT, 23, 24 and 25 Oct. These figures show that the southwesterly airflow was dominant in the domain, although an anti-clockwise circulation due to the low existed over England. The right, (d)-(f), are the predicted air concentrations at the ground level at T_0+24 (1600 GMT, 24 Oct.), T_0+48 (1600 GMT, 25 Oct.) and T_0+60 (0400 GMT, 26 Oct.). According to the predictions, the cloud of the tracer gas was transported eastward until T_0+48 and reached Poland. However, then, the eastward migration of the cloud was prevented and extended northward at Eastern Europe, where the convergence of easterly and westerly winds generated new airflows toward the north. **Figure 24** illustrates the final results, Set 6, that had been improved by the analyzed wind fields. Although no drastic change appeared when compared with the results of Set 1 shown in **Fig.23**, the discrepancies were seen in the extreme stretch of the cloud in **Fig.24(f)** at T_0+60. The air concentrations at ground level at T_0+60 for Sets 1 to 6 were compared in **Fig.25**. This shows the results for Sets 2 to 6 are resemble.

(2) Real-time response for Run 2

The progress with time of the near real-time response on Run 2 is shown in **Table 11**. Pre-alert information to make ready for near real-time predictions for the tracer release reached at 19:09, 13

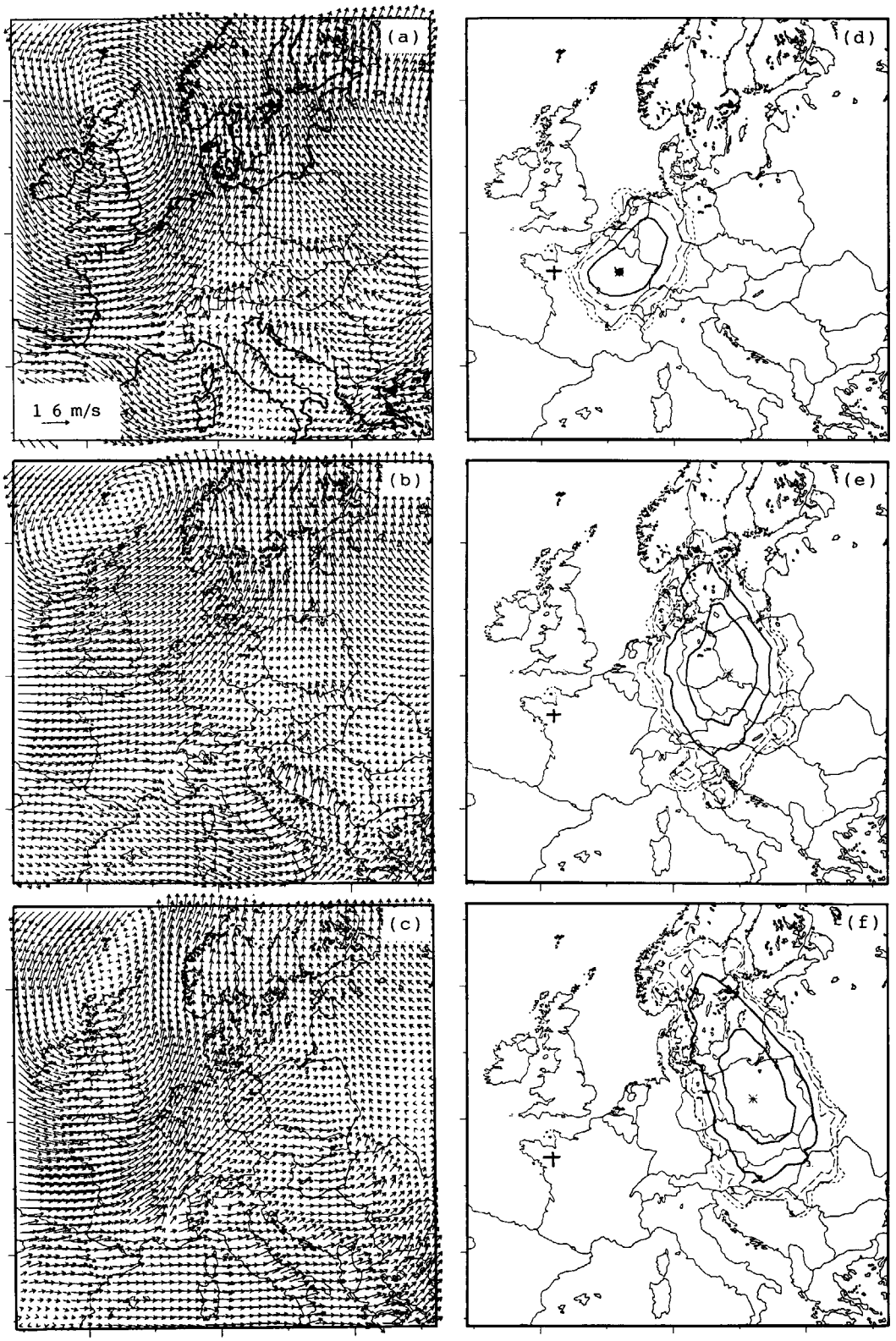

Fig. 23 The results of Set 1 in Run 1, which were based on the forecast data 23_12, Oct.; (a) - (c) : predicted wind fields near the surface at 1200 GMT, 23, 24 and 25 Oct., and (d) - (f) : predicted air concentrations at the ground level at T_0+24 (16 GMT, 24 Oct.), T_0+48 (16 GMT, 25 Oct.) and T_0+60 (04 GMT, 26 Oct.). The contour values are 10^{-1}, 10^{-2}, 10^{-3}, 10^{-4} and 10^{-5} ng/m^3 from the inside.

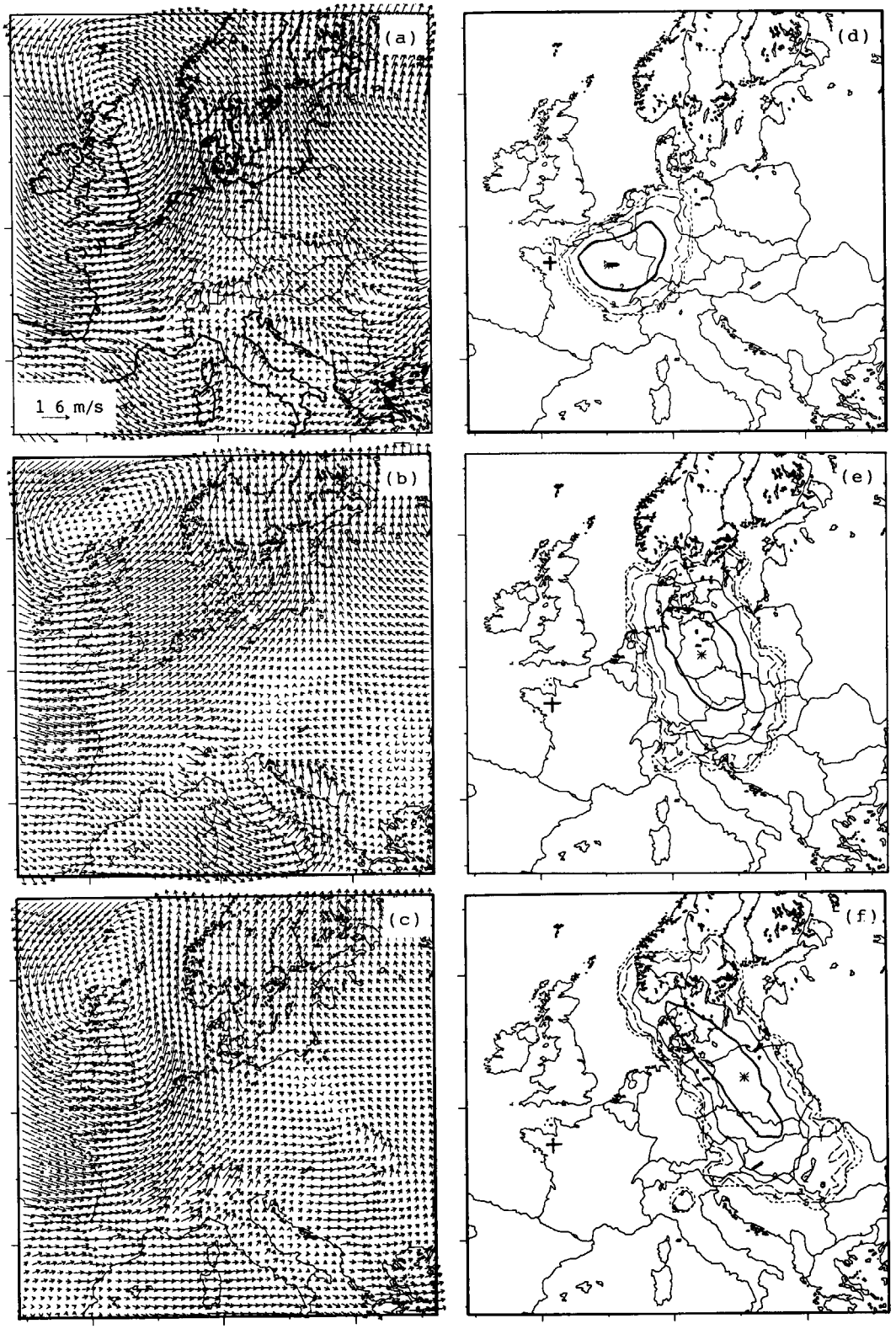

Fig. 24 The final results, Set 6 in Run 1, improved by analyzed wind fields.

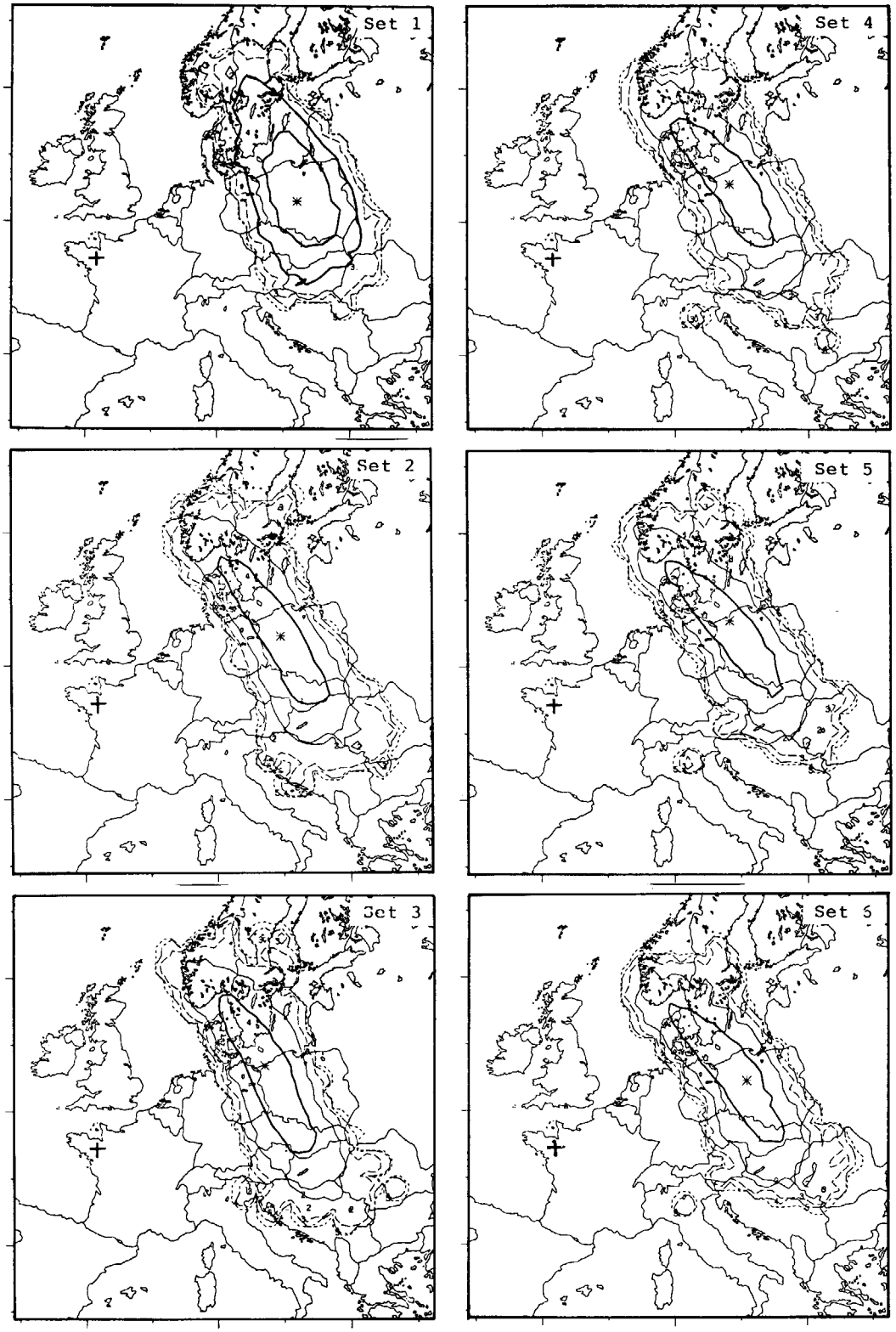

Fig. 25 Comparison of the air concentrations at the ground level at T_0+60 from sets 1 to 6.

Table 11 The progress with time of near real-time response on Run 2.

Date	Time (JST)	
13 Nov.	19 : 09	Pre-alert to inform the possibility of the tracer release within 32 hrs.
14 Nov.	14 : 00	Acquisition of the forecast data 14_00 and pre-calculation of wind field.
15 Nov.	00 : 21	Notification to inform the source term.
	00 : 40	Start of the air concentration calculation using the wind field based on the forecast data 14_00 and contour plots.
	02 : 30	Transmission of the predicted results to the ETEX evaluation team.
	03 : 00	Acquisition of the forecast data 14_12.
	03 : 05	Restart of the first prediction.
	04 : 20	Transmission of the revised predicted results to the ETEX evaluation team.
	14 : 27	Acquisition of the forecast data 15_00 and start of the second prediction.
	15 : 18	End of the second prediction.
16-17 Nov.		The third to sixth predictions.
18 Nov.		Transmission of all the predicted results to the ETEX evaluation team by INTERNET.

Nov. by facsimile and E-mail. The operation of WSPEEDI started from 14 Nov. The forecast data 14_00 were acquired at 14:00 and, subsequently, the wind field calculations by WSYNOP started in the afternoon of 14 Nov. The notification shown in **Fig.21** reached at 00:21 15 Nov. by E-mail, but the information by facsimile was delayed one hour and reached 01:20. This notification gave the release point in longitude and latitude, time of the release and its duration, release height and source strength. The tracer release, whose duration was 12 hours, started at 1500 GMT, 14 Nov. Since we had to wait for about two hours to acquire the new forecast data 14_12, we started the prediction of the tracer gas dispersion based on the forecast data 14_00, from which we had already calculated wind fields beforehand, the plotting of contours of air concentrations till 60 hours later and the transmission of the results to the ETEX evaluation team. This work could be finished within two hours, from 00:40 to 02:30, because of the quick prediction by the vector processor. The new data 14_12 were delayed being stored in the computer of ARL/NOAA, and became available to us at 03:00. Thus, the wind field calculations using the new data successively started at 3:05. We made a wind field and concentration calculations during the period from 3:05 to 4:50 and, subsequently, plotted nine figures, e.g., six wind fields every 12 hours for three days and the contours of the air concentrations at T_0+24, T_0+48 and T_0+60. Finally, the results requested were sent again to the ETEX evaluation team at 04:20 because 3 hours still remained until the time limit of the quick response by facsimile.

The response for the second set started at 14:27, 15 Nov. The predictions continued twice daily until 17 Nov. to improve the results using the last 72-hour forecasts from ARL/NOAA. The 6 sets of predicted results were sent to the ETEX evaluation team at 18 Nov.

The results of Set 1, which were based on the forecast data 14_12, are shown in **Fig. 26(a)-(f)**. The left, (a)-(c), are the predicted wind fields near the surface at 1200 GMT, 14, 15 and 16 Nov. The right, (d)-(f), are the predicted air concentrations at the ground level at T_0+24 (1500 GMT, 15 Nov.), T_0+48 (1500 GMT, 16 Nov.) and T_0+60 (0300 GMT, 17 Nov.).In this case, the wind speed was very high and a half of tracer cloud went out of the computational region after 60 hours. According to the wind fields near the surface, the cloud seemed to be transported to the northeast from Rennes, France. However, the predicted cloud flowed eastward, and then, southeastward after T_0+24. This is because

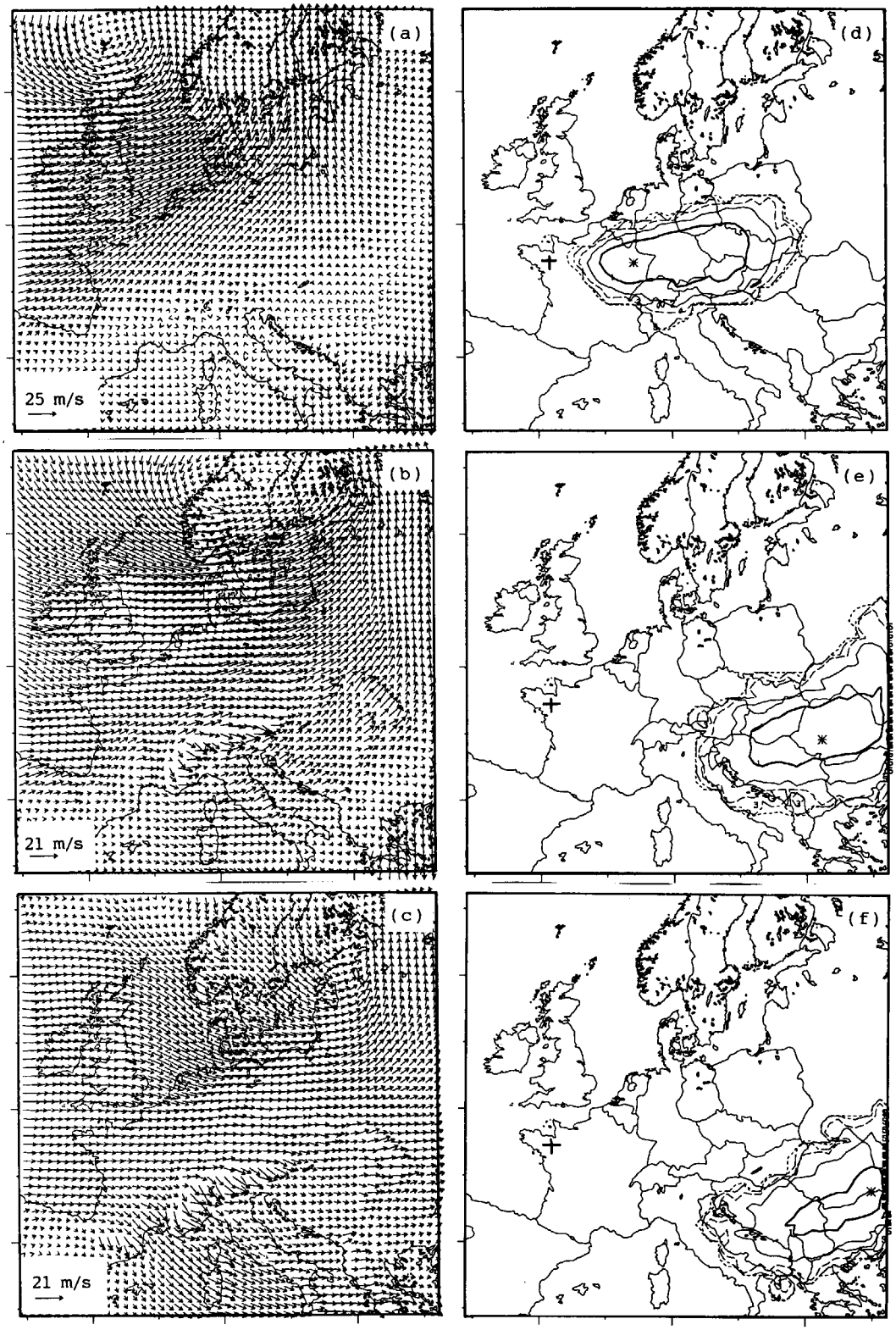

Fig. 26 The results of Set 1 in Run 2, which were based on the forecast data 14_12, Nov.; (a) - (c) : predicted wind fields near the surface at 1200 GMT, 14, 15 and 16 Nov., and (d) - (f) : predicted air concentrations at the ground level at T_0+24 (15 GMT, 15 Nov.), T_0+48 (15 GMT, 16 Nov.) and T_0+60 (03 GMT, 17 Nov.).

the upper wind fields in the boundary layer were different from those near the surface. **Figure 27** shows the wind fields at a height of 500 m above the ground at 0000 GMT, 16 Nov. This figure suggests that the cloud once dispersed upward due to turbulence were transported to the southeast by upper winds which represent the average wind in the boundary layer. It means that the upper wind in the boundary layer is critical for the long-range transport of materials even if the objective is the air concentration at ground level. **Figure 28** shows the final results, Set 6, improved by the analyzed wind fields. Because predicted wind speeds of Set 6 were smaller than those of Set 1, the main part of the cloud remained in the region in Set 6 and the concentration values were higher than those of Set 1.

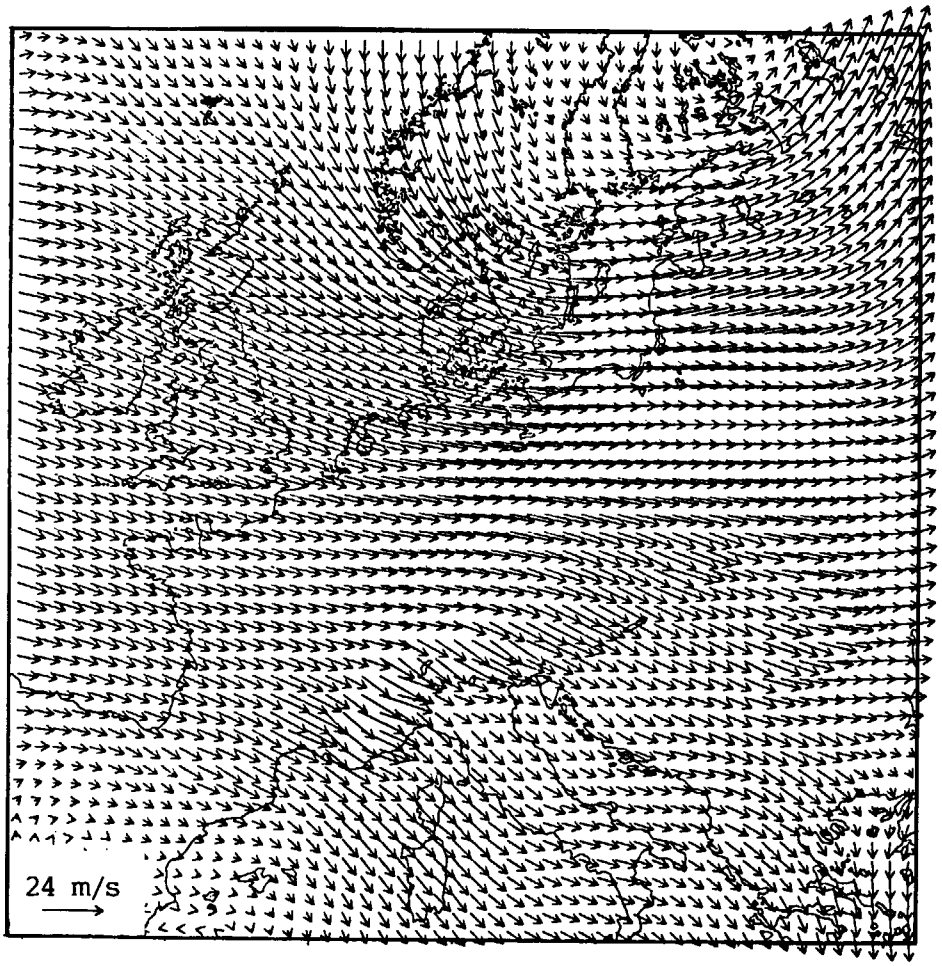

Fig. 27 Wind fields (Set 1) at a height of 500 m above the ground at 0000 GMT, 16 Nov.

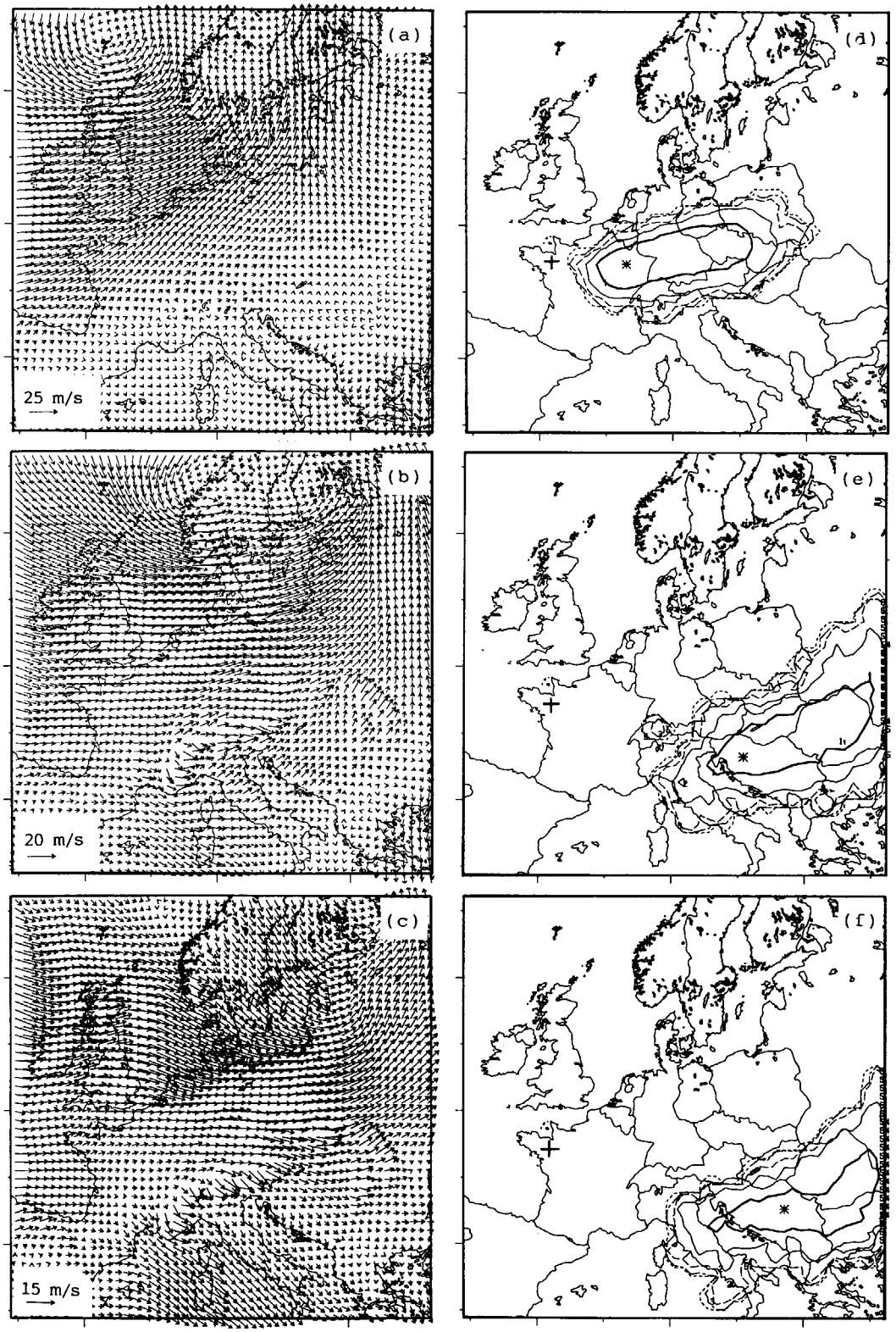

Fig. 28 The final results, Set 6 in Run 2, improved by analyzed wind fields.

4.2.3 Summary

The near real-time operation tests of WSPEEDI by participating ETEX, carried out twice, could accomplish all the tasks required by the ETEX evaluation team. Therefore, it could be verified that WSPEEDI has sufficient capability to respond to an accidental release of radionuclides from nuclear installations abroad, although it may not be valid that a presumed operation procedure, like this ETEX simulation, can be possible when information might be entangled during a real accident.

These experiences also revealed the problems to be solved when WSPEEDI is in practical use for a real accident in future. The time needed to acquire meteorological forecasts are critical for a quick response. In the ETEX application, we could get them from ARL/NOAA via INTERNET with about a 5 hour delay, for example, the data 23_00 came to the workstation of WSPEEDI at 05 GMT (14 JST), 23 Oct. However, the meteorological network now examined, mentioned in 3.3, needs 9 hours, because the data from JMA are once transmitted to JWA and, then, sent to the workstation of WSPEEDI, after the arrangement of data in the JWA. Thus, it is desirable to get forecast data from JMA directly via INTERNET or other high-speed communications services. Furthermore, since the global 30-hour forecasts are rather short in time for the prediction of the arrival of radionuclides discharged from Europe or the United States to Japan, a special service from JMA to provide WSPEEDI with the forecast in longer term is important.

Moreover, since WSPEEDI is now operated by researchers in the time-sharing system of the JAERI Computing and Information Systems Center, and consequently affected by the congestion of jobs, maintenance, etc., it will be needed to have an exclusive computer system and operators for WSPEEDI to maintain a 24-hour service system.

5. Concluding Remarks

The ultimate goal of the development of WSPEEDI is to provide a practical computer code system for the rapid prediction of various types of information on radiation levels, radioactive concentration and radiological impact on Japanese under the situation of an accidental releases from a nuclear facility abroad. Thus, WSPEEDI is required to simulate the long-range transport of radionuclides up to the hemispheric scale and the top of the troposphere (~ 10 km) in the vertical dimension. The design and development of WSPEEDI have been carried out to meet these necessities. The current status is summarized below.

WSPEEDI is implemented on a computer network. The primary computers in the network are two front-end workstations ΛΣ340, Fujitsu Ltd., Japan, for data communications and graphical outputs and multipurpose computers M780 and VP2600, Fujitsu Ltd., both installed at the JAERI Computing and Information Systems Center. These computers are connected by the Local Area Network (LAN) of JAERI and the data communications workstation also has a line to the Japan Weather Association (JWA) to acquire meteorological information.

The software WSPEEDI consists of the physical models WSYNOP/GEARN and system modules to support the operator for quick response. A mass-consistent wind model, WSYNOP, is for predicting large-scale 3-D wind fields every 6 hours by using worldwide meteorological observed data or global meteorological forecast data provided by the Japan Meteorological Agency (JMA). A particle random walk model, GEARN, predicts atmospheric transport, deposition on the ground and radiological doses to the public using 3-D wind fields provided by WSYNOP, source term and geography. These models can take account of the complex source, terrain conditions, and non-uniform and non-steady atmosphere. Although the models are basically the same as those of SPEEDI, several points have been improved for long-range transport, e.g., the coordinates, consideration of atmospheric density and precipitation distribution, etc.

For easy operation of computational codes in emergency situations, the WSPEEDI codes are systematised in combination with the system modules, e.g., the system control software, meteorological data processor, databases and graphic software.

The global meteorological forecasts out to 30 hours (GPV) are designed to be transmitted twice daily from JMA via JWA to the communications workstation which has the meteorological data processor. These data are decoded, formatted and sent to M780.

The M780 computer contains the system control software and databases which include invariant data, e.g., worldwide geographical data, site data, etc. The operator can easily initiate a WSPEEDI response with a choice of command that generates the questionnaire to be displayed on user-friendly menus and then prompts the operator to input accident information such as time, location, and type of release and so on. Release information is inputted in near real-time from the keyboard. The operator typically carries out twice-daily forecasts on the transport of radioactive materials out to 30 hours just after new GPV meteorological data become available.

The calculations by WSYNOP/GEARN are carried out in a vector processor, VP2600, under the control of M780. At the same time, near real-time data, e.g., source term and meteorological data, and data from the databases are also sent to VP2600. The computer programs of WSYNOP/GEARN are rewritten in a form suitable for vector processing. The typical CPU times for the calculations of six 3-D wind fields and the transport of materials for three days are, in the case of ETEX, about 200 and 90 sec for WSYNOP and GEARN, respectively.

The predicted results, e.g., wind fields, airborne concentrations, deposition, external γ doses and

internal doses by inhalation are output into the files on the M780 computer and the operator can generate a variety of graphical outputs on the graphic workstation in the form of wind vectors or contours superimposed on a map.

The performance of the models has been evaluated using the Chernobyl case with reliable source terms, well-established meteorological data and a comprehensive monitoring database. Furthermore, the response of the system has been examined by near real-time operation for European Tracer Experiment (ETEX), carried out in about 2,000 km area of Europe. The results suggest that the combination of WSYNOP/GEARN works well as a computer model for the estimation of the long-range transport of radioactivity. Furthermore, the application of WSPEEDI for the near real-time operation for ETEX showed that the capability of WSPEEDI is sufficient to make forecasts during an emergency and, at the same time, the tasks to be solved in practical use are found.

WSPEEDI is currently close to satisfying the practical needs for near real-time estimation of environmental situations in an emergency.

Future studies to improve the reliability of the predicted results are, (1)consideration of spatial and temporal variation of the mixed layer, (2)sensitivity analysis of main parameters using the ETEX experimental data and (3)definition of appropriate resolution of computational mesh according to the objective regions.

The following problems must be also solved for the practical use. The meteorological data acquisition system of WSPEEDI is still in the testing stage. However, beginning in Spring 1995, the Japan Meteorological Agency routinely releases analyzed and forecast data on various scales, called GPV(Grid Point Values). Thus, it is an urgent task to establish a practical computer connection with an agency which is in charge of distributing GPV data. In particular, it is desirable to acquire forecasts over the Asian area with finer resolutions, compared with the global data, to simulate the influence on Japanese people due to a nuclear accident in neighboring countries. Furthermore, since the global 30-hour forecasts are rather short in time for predicting the arrival of radionuclides discharged from Europe or the United States to Japan, a special service from the JMA to provide WSPEEDI with the forecast over a longer term is important.

Moreover, it will be needed to have an exclusive computer system and operators for WSPEEDI to maintain a 24-hour service system.

Acknowledgment

The authors would like to express their sincere thanks to the members of the following committee, international and national organizations and institute, whose advice and assistances have made the construction of WSPEEDI much easier.

JAERI committee on Environmental Radiation Research (Dr. Jiro Kondo, Chairman) for control and guidance of the research project including the construction of WSPEEDI.

The Japan Meteorological Agency and the Japan Weather Association for providing the GPV data during the testing period of the WSPEEDI data communications lines.

The European Commission (former Commission of the European Communities (CEC)), the World Meteorological Agency (WMO) and the International Atomic Energy Agency (IAEA), who sponsored the ATMES and ETEX projects and kindly invited WSPEEDI to participate in these projects.

Dr. Roland Draxler of the National Oceanic and Atmospheric Administration (NOAA) of the U.S. for providing meteorological forecast data from NOAA during the ETEX project.

The National Center of Atmospheric Research (NCAR) of the U.S. for providing the U.S. Navy Global 10 Minute Elevation Data.

The members of the JAERI Computing and Information Systems Center (Dr. Masayuki Akimoto, Head) for their assistances through the development of WSPEEDI, in particular, Messrs. Takayuki Yamada and Mineyoshi Tomiyama for construction of a data communication line and for assistance during the near real-time test for ETEX, respectively.

References

(1) Japan Nuclear Safety Commission : Report on Countermeasures Against a Nuclear Accident, Japan Nuclear Safety Commission Tokyo, (1975) (in Japanese).
(2) Japan Nuclear Safety Commission : Guideline for Emergency Monitoring, Japan Nuclear Safety Commission Tokyo, (1984) (in Japanese).
(3) Chino, M., et al.: Rad. Prot. Dos., 50, 145, (1993).
(4) Science and Technology Agency of Japan: SPEEDI, pamphlet, Nuclear Safety Technology Center Tokyo, (1994)
(5) Zentralanstat fur Meteorologie und Geodynamik: Proc. of Int. Mtg. of EURASAP, Osterreichishe Beitrage zu Meteorologie und Geodynamik Wien, (1989).
(6) Klug, W., et al. (ed) : "Evaluation of Long Range Atmospheric Transport Models using Environmental Radioactivity Data from the Chernobyl Accident", (1992), Elsevier Sci. Publ.
(7) Chino, M., et al.: JAERI-M 86-142, (1986).
(8) Ishikawa, H.: J. Applied Meteor., 33, 6, (1994).
(9) Ishikawa, H., Chino, M.: J. Nucl. Sci. Technol, 28, 642, (1991).
(10) Sherman, C.A.: J. Appl. Meteor., 17, 312, (1978).
(11) Ishikawa, H.: J. Nucl. Sci. Technol., 28, 535, (1991).
(12) Kitada, T.: Atmos. Environ., 21, 785, (1987).
(13) Moussiopoulos, N., et al.: J. Appl. Meteor., 25, 847, (1986).
(14) Gifford, F.A.: Atmos. Environ., 16, 505, (1982).
(15) Ahlstrom, S.W., et al.: BNWL-2127, 111, (1977).
(16) Diehl, S.R., et al.: J. Appl. Meteor., 21, 69, (1982).
(17) Minato, S.: Isotope, 40, 1, (1991).
(18) Sehmel, D.A.: Atmos. Environ., 14, 983, (1980).
(19) Brenk, H.D., et al.: Nucl. Safety, 22, 362, (1981).
(20) Poston, J.W., Snyder, W.S.: Health Physics, 26, 287, (1974).
(21) Kocher, D.C., Sjoreen, A.L.: ibid., 48, 193, (1985).
(22) Kai, M.: Hoken Butsuri, 18, 3, (1983) (in Japanese).
(23) ICRP: ICRP Pub.23, Pregamon Press Oxford, (1975).
(24) Hofmann, W., et al.: Health Physics, 37, 517, (1979).
(25) ICRP: ICRP Pub.30, Pregamon Press Oxford, (1979-1982).
(26) CEC, WMO, IAEA: ETEX, pamphlet, (1994).
(27) INSAG: "Summary Report on the Post-Accidental Review Meeting on the Chernobyl Accident", IAEA Vienna, (1986).
(28) Salo, A.: IAEA BUll., 28, 18, (1986).
(29) Sinnko, K., et al.: STUK-A56, (1987).
(30) Jensen, M., Lindhe, J.C.: IAEA Bull., 28, 30, (1986).
(31) Aarkrog, A., et al.: Riso-R-549 (ISSN 0106-2840), (1987).
(32) Henriksen, T., et al.: OUP-87-24 (ISSN 0332-5571), (1987).
(33) Jagielak, J., et al.: Rad. Rrot. Dos., 20, 243, (1987).
(34) Jaworowski, Z., et al.: J. Environ. Radioactiv., 6, 145, (1988).
(35) Pienkowski, L., et al.: J. Radioanal. Nucl. Chem., 117, 379, (1987).
(36) Giacomelli, R., et al.: RT/COMB/86/4 (ISSN 0393-6252), (1986).
(37) Andrasi, A., et al.: KFKI-1986-49/K (ISSN 0368-5330), (1986).
(38) Hotzl, H., et al.: Rasiochem. Acta, 41, 181, (1987).

(39) Deworm, J.P. (ed.): BLG-595, (1987).
(40) Cambray, R.S., et al.: Nucl. Energy, 26, 77, (1987).
(41) CEA-ISPN-2, (1986).
(42) Arkrog, S., et al.: Riso-M-2692, (1986).
(43) Ishikawa, H.: J. Appl. Meteor., in press.
(44) Giacomelli, R., et al.: RT/COMB/86/6 (ISSN 0393-6252), (1986).
(45) Anttila, P., et al.: J. Aerosol Sci., 18, 939, (1987).
(46) Draxler, R.R., Heffter, J.L. (eds.): NOAA Technical Memorandum ERL ARL-167, (1989).
(47) Chino, M., et al.: J. Nucl. Sci. Technol. of Jpn, 37, 312, (1995) (in Japanese).